Nano Today 44 (2022) 101501

Contents lists available at ScienceDirect

Nano Today

journal homepage: www.elsevier.com/locate/nanotoday

Review

Research progress on penta-graphene and its related materials: Properties and applications

Muhammad Azhar Nazir, Arzoo Hassan, Yiheng Shen, Qian Wang*

School of Materials Science and Engineering, CAPT, Peking University, Beijing 100871, China

ARTICLE INFO

Article history:
Received 26 February 2022
Received in revised form 11 April 2022
Accepted 29 April 2022
Available online 12 May 2022

Keywords:
Penta-graphene
Negative Poisson's ratio
Nano-auxeticity
Piezoelectricity
Heterojunction

ABSTRACT

The most direct and efficient strategy in designing and synthesizing new materials is to change the structural building units, which could lead to a new paradigm shift. Penta-graphene (PG) is such an example where the structural unit is pentagon rather than hexagon as in graphene. Since we proposed the unique structure of penta-graphene, a two-dimensional (2D) carbon allotrope entirely composed of carbon pentacyclic rings [*Proc. Natl. Acad. Sci. U. S. A.* 112, 2372 (2015)], tremendous efforts have been made to explore the novel properties of PG and its derivatives such as penta-nanotubes, penta-nanoribbons, multilayer PG, functionalized PG, and polycrystalline PG. These materials exhibit novel physical and chemical properties, including nano-auxeticity, intrinsic piezoelectricity, ferroelectricity, spontaneous polarization, and catalysis, showing great potential for the applications in battery anode, spin-splitting/filtering, gas separation, biodetection, and heterojunctions. More importantly, PG has inspired a lot of efforts in the design and synthesis of other pentagon-based 2D materials with exceptional properties and promising applications (http://www.pubsd.com/). In this paper, we provide a comprehensive review on the progress made in this new field by focusing on the structure-property relationship. We discuss the main achievements that have provided an in-depth understanding of the novel properties and applications of pentagon-based materials, ranging from PG to PG derived materials, and PG's cousins (penta-silicene and penta-germanene). This review can not only help to better understand the property evolution of the elemental penta-sheets in the same group, but also provides a bird's eye view on how the structural unit changes the functionalities of materials.

Contents

Abbreviations: CNT, Carbon nanotube; PG, Penta-graphene; AIMD, Ab initio molecular dynamics; DFT, Density functional theory; NPR, Negative Poisson's ratio; LDA, Local density approximation; GGA, Generalized gradient approximation; DOS, Density of states; TB, Tight-binding; DNA, Deoxyribonucleic acid; MC, Monte Carlo; SAC, Single-atom catalyst; STM, Scanning tunneling microscopy

* Corresponding author.
E-mail address: qianwang2@pku.edu.cn (Q. Wang).

https://doi.org/10.1016/j.nantod.2022.101501
1748-0132/

Introduction

The bonding flexibility and unique electronic configuration extend the credibility of carbon atoms to form an ever-expanding library of colorful allotropes with all dimensions [1,2]. Particularly, ranging from 3D graphite to 2D graphene [3], 1D carbon nanotubes (CNTs) [4], and 0D fullerenes [5], hexagons are the most dominant building blocks of the carbon family [6]. Among these, hexagonal graphene has been of great interest in the materials community due to its novel 2D atomic structure and potential applications in optoelectronics, photo-detectors, supercapacitors, spin filtering, and energy storage devices [7]. Despite the fascinating characteristics, the semi-metal (zero bandgap) behavior of graphene significantly hampers its direct uses in nano electronic devices and nanotechnology [8]. Consequently, this concern has motivated many more theoretical and experimental studies for the bandgap tunability [9–13], but still, at the same time, researchers are tirelessly exploring alternative materials to graphene with rich physics, intrinsic bandgap, and a wealth of unusual properties.

The central motive in modern materials research is to tune the structure-property relationship that mainly depends on the configuration, composition, and shape of structural building blocks. Rational manipulation of structural blocks can lead to a new class of novel materials with enhanced properties and device performance. As a result, much effort has been devoted to seeking highly suitable geometric blocks to form novel materials beyond conventional hexagons.

Herein, we focus on pentagonal building blocks because they have attracted tremendous attention in the domain of mathematics and materials science due to their unique structural motifs and attractive pentagonal tiling patterns. Historically, the concept of pentagons dates back to the nineteenth century with the pioneering work of the German mathematician Karl Reinhardt in 1918 [14] on using irregular pentagons to tile the Euclidean plane. Till date, 15 types of irregular pentagons that can tessellate a plane, leaving no gaps and without overlaps, have been discovered [15–17], and the last one was found in 2015 [18]. The new solution for M.C. Escher-like puzzle is inspiring; however, the realization of these mathematical models in materials is challenging. The design and synthesis of pentagonal materials strongly demand flexibility in the bonding and hybridization of elements in the periodic table. In this scenario, carbon emerged as the first choice of researchers as it can form a single bond, double bond, and triple bond, and can be in *sp*, sp^2, and sp^3 various types of hybridization. In addition, the successful isolation of C_{20} fullerene, which is purely composed of 12 pentagons [19], has also fueled the availability of other low-dimensional pentagonal materials.

Based on extensive computational simulations, in 2015, we proposed penta-graphene (PG), a 2D carbon allotrope composed of only pentagons [18]. More interestingly, we found that from PG, many other pentagon-based structures can be constructed. For instance, various fused-pentagon-based nanotubes, and penta-tubes were made by rolling up PG sheets, and different 3D pentagon-based stable crystal structures were built by stacking PG sheets in different patterns [18]. PG has received considerable attention because of its unique geometric structure and novel properties. Many follow-up works on PG-derived structures have been reported, including PG nanoribbons [6,20–22], double-layer PG [23], multilayer PG [23], and surface modification of PG [24,25]. Further studies on the physical properties of PG have also been performed. For instance, GW and Tight-binding approaches were applied to revisit the band structure of PG [26,27]. The mechanical [18,28], optical [29], piezoelectric [30], and thermal transport properties [31,32] of PG have been systematically studied. The intriguing properties of PG make it promising for vast applications, including as a metal-free catalyst for CO oxidation [33], a hydrogen storage material [34], a piezoelectric material [30], an anode material for Li-ion batteries [35], and as a channel material in heterojunctions for the field-effect transistor [36]. More importantly, the proposal of PG has motivated the research on binary and ternary pentagon-based 2D materials on theoretical and experimental grounds [37–47]. Based on the atomic configuration of PG, many such pentagon-based 2D materials have been predicted,

and some of them have been experimentally synthesized [48], including penta-silicene nanoribbons [46], penta-$PdSe_2$ [49], and penta-NiN_2 [50]. Obviously, PG provides a novel structural model for new 2D materials going beyond the conventional sheets such as graphene, MoS_2 and black phosphorus.

Inspired by these findings, this review strives to present an exciting journey of pentagonal materials from theoretical prediction to practical realization. Thus, the sections of this review are organized as follows. The detailed geometric configuration and stability of PG (being a mother structure) are expounded in section *Geometry and stability of PG*. The mechanical, electronic, optical, and thermal transport, adsorption, and catalytic properties of PG, and its potential applications in H_2 storage, CO_2 capture, heterojunctions, gas sensor, and Li-ion batteries are reviewed in section *Properties and applications of PG*. In section *PG derived structures*, the derived structures from PG, including penta-nanotubes, penta-nanoribbons, multilayered PG, functionalized PG, and 3D diamond-like pentagon-based structures, are discussed. In section *The cousins of PG*, an extension of the discussions is made to the cousins of PG, namely, penta-silicene and penta-germanene. Finally, in the last section, a comprehensive summary combined with the latest research advances is provided to enrich the critical concepts in this emerging field and the challenges for the future study. This review would pave the way for those who are exploring the fundamentals of this new but quickly expanding family of pentagon-based materials.

Geometry and stability of PG

Carbon started its pentagon-based journey in 1952 with the discovery of the pure pentagonal molecular structure "cyclopentadiene" [51]. After the complete silence of 45 years, new signs of progress were made in this field with three structures, including two molecular structures composed of two and three carbon five-membered rings, named pentalene [52] and acepentalene [53], and the zero-dimensional molecule, C_{20} fullerene [19], as sketched in Fig. 1a. While due to the high stability of hexagons in carbon allotropes, the non-hexagonal (pentagonal or heptagonal) carbon structures were generally considered as geometrical frustrations or topological defects in materials [54]. Surprisingly, the prediction of PG changed all these thoughts in the scientific community and glorified the performance of unique pentagons in materials [18]. More importantly, its purely pentacyclic morphology firmly nominated pentagons as important structural units of the carbon family beyond traditional hexagons.

Since the prediction, PG has become one of the most hotly studied materials among group-IV elements. The structural novelty of PG has spellbound the research community and triggered a strong resurgence of interest in developing/synthesizing numerous pentagonal materials. According to the updated database for 2D pentagonal materials [48], more than 100 reports inspired by PG have discussed the physical and chemical aspects of the various pentagonal sheets, and this number remains quickly growing. In this light, this section enlightens PG's structural characteristics and stability.

Initially, one of the early motivations for exploring pentagonal materials was to investigate the detailed geometrical properties of PG and how PG could provide unusual properties and performance differing from graphene. In this domain, advanced computational simulations have made significant progress and enabled scientists to explore the in-depth picture of material in a more efficient manner. Consequently, numerous studies have reported the detailed geometrical features of PG in literature [8,55–58], while instead of reviewing the entire literature, this review mainly highlights the basic geometric pattern of PG to reflect its unique appearance in materials science.

Theoretically, it is manifested that a monolayer PG sheet can be chemically exfoliated by breaking interlayer covalent bonds of bulk T12-carbon (Fig. 1b) [18,23,29,59] and belongs to $P42_1m$ symmetry and space group No. 113 [18]. As schematically shown in Fig. 1c, an ideal PG structure can be constructed by repeating identical five-membered carbon building blocks in two dimensions, which reminds the beautiful tessellation patterned in the type-II pentagonal tiling that resembles the Cairo tiling. Geometrically, PG's unit cell (highlighted by the solid square in Fig. 1c) comprises six carbon atoms in three sublattices, including two four-fold coordinated and four three-fold coordinated atoms (called C1 and C2, respectively), forming a sandwich-like structure [18]. Symmetrically, C1 atoms construct the middle plane at $z = 0$, and C2 atoms form both outer planes at $z = \pm h$, where h is the distance between the top/bottom layer and the middle plane of PG [18,60]. More importantly, the uniqueness of PG exists in its hybrid nature of non-equivalent chemical bondings, such as the slightly longer single bond between C1–C2 and the marginally shorter double bond between C2–C2. Interestingly, the existence of tetrahedral sp^3 bonds leads to buckling of ~ 0.6 Å (side view), resulting in the total thickness of ≥ 1.2 Å in this sheet [18,55,61,62]. As a result, the advent of purely buckled configuration induces non-planarity in PG and characterizes it as a quasi-2D sheet [18,24].

Besides the geometric aspects, the theoretical prediction of a novel material enormously concerns the stability and synthesis of this material. Usually, the relative stability of the proposed structure is governed by energetics, thermo-dynamics, and mechanics. Computationally, Zhang et al. [18] reported the thermodynamical stability of PG by performing phonon dispersion calculations and ab initio molecular dynamics (AIMD) simulations from room temperature (300 K) to high temperatures of 1000 K. As shown in Fig. 1d, four optimized PG supercells retain their pentagonal periodicity at different temperature intervals, confirming the thermal stability of PG up to 1000 K. Moreover, the absence of negative frequencies (imaginary modes) in the phonon spectrum reveals the dynamical stability of PG (Fig. 1e) [18]. Although the total energy calculations indicate the metastability of PG as compared to graphene [18,63,64], still, it is found more stable than some successfully synthesized structures, i.e., T-carbon [65], C_{20} [66], and cyclo carbon sheet [67], etc. One of the challenges of synthesizing the PG sheet is to get a suitable precursor. For example, Zhang et al. [18] have shown via AIMD simulations in their pioneer work that the addition of H_2 molecules to a 4-layer (001) thin film of T12-carbon may tend to break the C—C bonds and could lead to the exfoliation of a partially hydrogenated PG sheet from T12-carbon. And consequently, the PG sheet can be obtained via the dehydrogenation process. Despite numerous theoretical indicatives, the scientific community is still waiting for viable routes to synthesize monolayer PG.

Properties and applications of PG

The increasing literature on pentagonal materials clearly indicates that they have captured significant attention from various research communities, including material scientists, physicists, chemists, and bio-specialists, due to the fascinating properties and many potential applications of PG. Particularly, being a mother structure of the pentagonal family, the initial motivation was to investigate the fundamental properties of PG, which could enable scientists to design/synthesize other novel pentacyclic materials with tailored collective properties that have never been seen in nature. Many of its properties, including mechanical, optoelectrical, thermal, etc., are intimately tied to its pentagon-based morphology, hybrid atomic bonding nature, and highly tunable surface chemistry. Furthermore, all the subjected properties of PG can be tuned by controlling its surface modification under different functionalities, e.g., temperature variations [68], strain engineering [23], chemical functionalization [24] and chemical doping [69], etc., which would result in intriguing prospects/opportunities for PG in materials

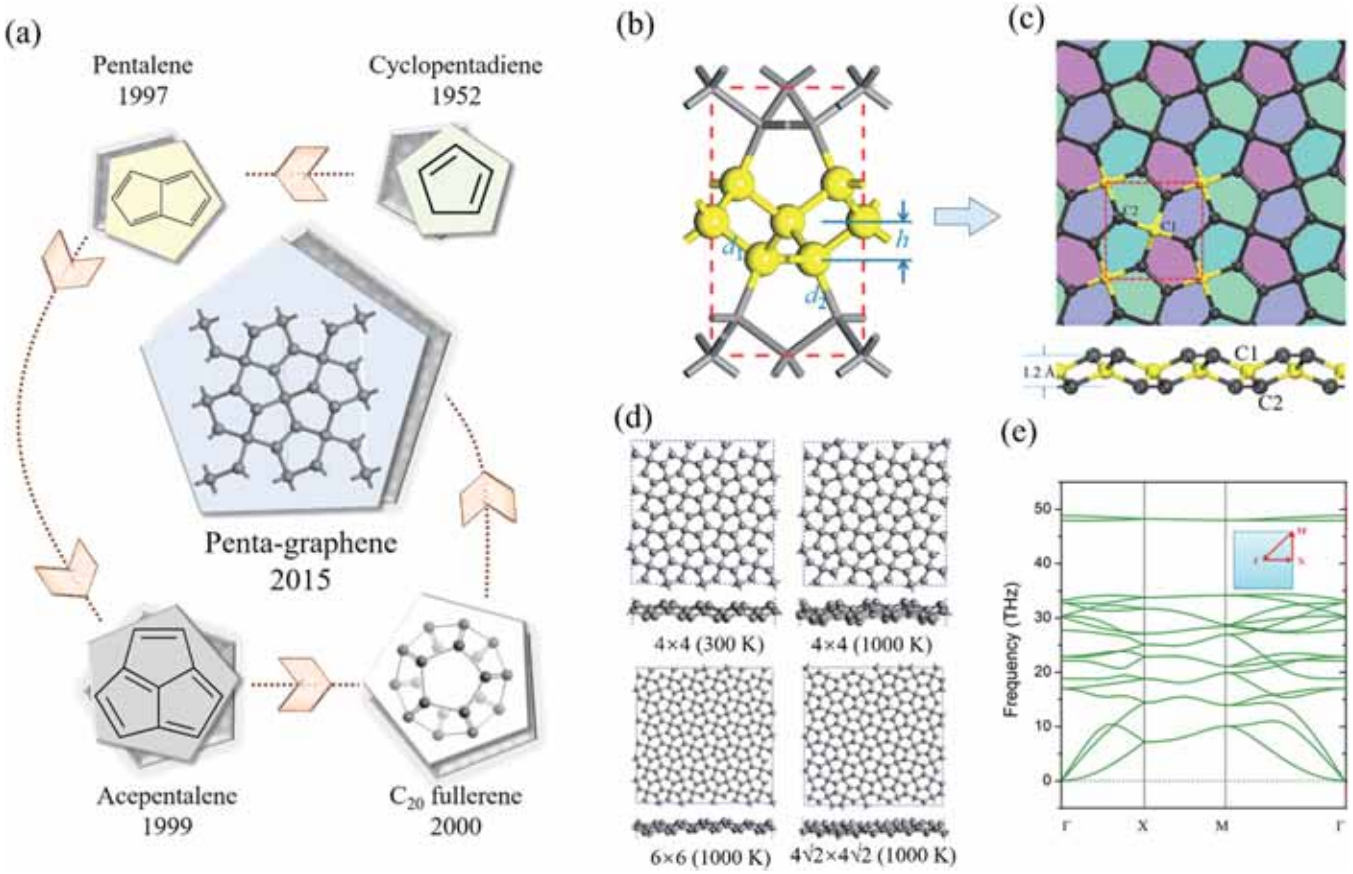

Fig. 1. (a) Pentagonal evolution of carbon structures from cyclopentadiene to PG. (b) Optimized crystal structure of T12 carbon viewed from the [100] direction. (c) Top and side views of the geometric structure of PG with a 2 × 2 supercell. (d) Optimized structures of PG with different supercells and temperatures. (e) Phonon band structure of PG along the highly symmetric q-paths.
(b–e) Adapted with permission from Ref. [18]. Copyright 2015, National Academy of Science.

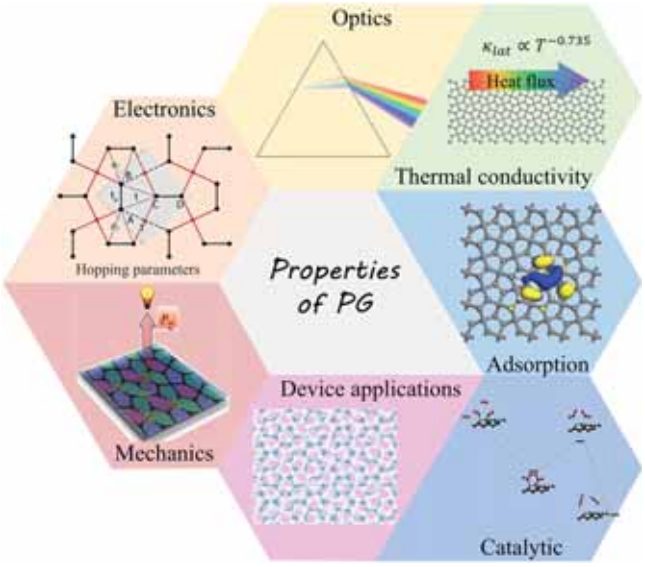

Fig. 2. An overview of the properties and applications of PG.
Illustration for "Electronics" is adapted from Ref. [27]. Illustration for "Adsorption" is adapted with permission from Ref. [70]. Copyright 2020, Elsevier. Illustration for "Catalytic" is adapted with permission from Ref. [167]. Copyright 2018, Royal Society of Chemistry. Illustration for "Device applications" is adapted with permission from Ref. [36]. Copyright 2017, American Institute of Physics. Illustration for "Mechanics" is adapted with permission from Ref. [18]. Copyright 2015, National Academy of Science.

science. In consideration of this motivation, this section not only summarizes the detailed properties of PG but also highlights its impressive potential in various applications such as piezoelectric devices, energy storage, biosensor, catalysis, and heterojunctions, as sketched in Fig. 2.

Mechanical properties

Up to date, the in-plane mechanical properties of the monolayer PG have been well investigated by multiple groups and reported in literature [18,28,71–76]. The mechanical parameters of PG, such as elastic constants, Young's modulus, and Poisson's ratio, as listed in

Table 1
Summary of the elastic constants (C in GPa·nm), Young's modulus (E in GPa·nm), and Poisson's ratio of PG, graphene, H-PG, H-GR, F-PG and F-GR.

System	C_{11}	C_{12}	C_{66}	E	ν	Ref.
PG	265	−18	152	263.8	− 0.068	[18]
	267.54	−18.81	150.95	266.22	− 0.070	[76]
	270.2	−17.6	151.8	269.03	− 0.065	[71]
	271.84	−20.86	153.15			[80]
	275.7	−21.43		278.0	− 0.078	[28]
					− 0.08	[72]
	277.5	−26.7		274.95	− 0.096	[8]
				376 ± 13.6		[74]
Graphene				342 ± 30		[75]
H-PG	224.2	44.3	152.9	215.4	0.197	[71]
	218.4	53.13		205.50	0.243	[24]
H-GR				243	0.07	[79]
F-PG	253.2	59.70		239.12	0.236	[24]
F-GR				226	0.10	[79]

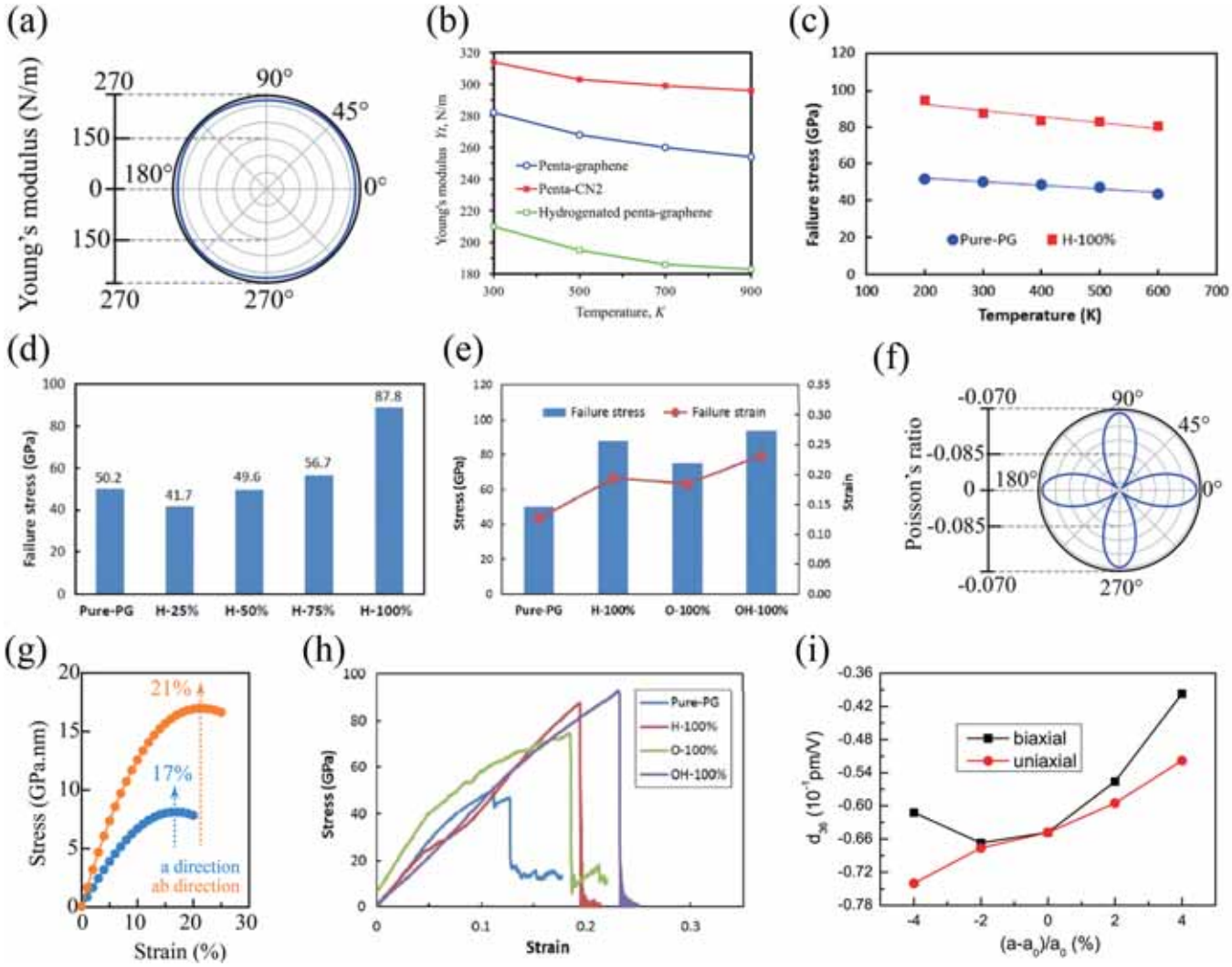

Fig. 3. (a) Angle-dependent Young's modulus of PG. (b) Effect of temperature on the Young's modulus of PG and H-PG, and (c) on failure stress of PG and H-PG with 100% coverage of hydrogen. (d-f) Failure stress of PG with different hydrogen coverages. (e) Failure strain of chemically functionalized PG with 100% coverages of H, O, and OH groups. f) Angle-based Poisson's ratio of PG. g) Stress-strain relationships for PG under the uniaxial strain along with the *a* direction and biaxial strain along the *a* and *b* directions. h) Stress-strain curves for pristine PG and the functionalized PG with 100% coverages of H, O, and OH groups. i) Predicted piezoelectric constant (d_{36}) for PG under the effect of uniaxial and biaxial strains.

(a, f, g) Adapted with permission from Ref. [76]. Copyright 2021, American Physical Society. (b) Adapted with permission from Ref. [68]. Copyright 2017, Elsevier. (c-e, h) Adapted with permission from Ref. [25]. Copyright 2017, Springer. (i) Adapted with permission from Ref. [80]. Copyright 2020, Elsevier.

Table 1, play a significant role in predicting PG's mechanical stability and strength under various conditions. The results in Table 1 imply that the elastic constants meet the requirements of mechanical stability under equilibrium conditions, namely, $C_{11} > |C_{12}|$ and $C_{66} > 0$ [18]. Theoretically predicted Young's modulus of PG reflects isotropic behavior (Fig. 3a) and quite comparable stiffness to that of graphene [74]. Notably, the in-plane stiffness of PG can be attributed to its pentagonal atomic configuration and the emergence of strong covalent bondings between carbon atoms.

The mechanical properties of PG can be tuned by introducing dopant, defect, and surface modifications, as reported in some earlier studies [25,68,74,77]. For example, Le [68] predicted the reduction of Young's modulus (Fig. 3b) of PG as a function of increasing temperature from 300 K to 900 K. Han et al. [73] observed a significant reduction in the Young's modulus of PG as increasing strain. Zhang et al. [25] calculated the values of failure stress and failure strain of pristine PG to be 50.2 GPa and 0.127, respectively, which are much lower than those of graphene, as reported experimentally (130 GPa and 0.25) by atomic force microscopy [75] and theoretically (125.2 GPa and 0.191) by MD simulations [78].

In this regard, chemical functionalization, including assisted PG sheet with hydrogen (H), fluorine (F), epoxide (–O–), and hydroxyl (-OH) groups, has been found to be a very effective strategy for tuning mechanical properties of PG. For example, Le [68] showed that hydrogenated PG (H-PG) offers higher stiffness than the pristine PG sheet, and increasing temperature reduces Young's modulus by only ~25–28% even at 900 K (Fig. 3b). This reduction is attributed to the pre-stretching of C2—C2 carbon bonds and increased buckling distance between PG layers after hydrogenation. Interestingly, it was also reported for hydrogenated graphene (H-GR) that hydrogenation reduces its Young's modulus even at 300 K, and the similar trend was found for fluorinated graphene (F-GR) as well [79]. From this point of view, PG and graphene share one feature in common, namely, both hydrogenation and fluorination reduce their Young's moduli, as listed in Table 1, whereas the values of Poisson's ratio for these functionalized GR sheets are much lower than those of the functionalized PG. Besides, density functional theory (DFT) calculations have found that the complete functionalization (with 100% coverage) improves structural stability, failure stress, failure strain, and tensile stress of PG but reduces its Young's modulus at the same time

[24,25,68]. Zhang et al. [25] have also shown that although increasing temperature (200–600 K) reduces failure stress (Fig. 3c), but H-PG (with 100% coverage) still offers ~71–88% higher values than that of the pristine PG. More precisely, PG's failure stress and strain can be enhanced up to 86.6% and 82.4% after functionalizing the PG sheet with OH species rather than the other two groups (Fig. 3d-e) [25].

Negative Poisson's ratio

Negative Poisson's ratio (NPR) refers to the ability of an auxetic material to become wider (rather than shrink) in its lateral direction under the application of uniaxial tensile strain. Mechanically, the uniqueness of PG mainly arises from its negative Poisson's ratio (Fig. 3f), resulting from the negative value of the C_{12} constant [18,28,71,72], as summarized in Table 1. This implies that if stretched on one axis, PG will expand on the axis perpendicular to it as well. Generally, most natural materials expand in the same direction and contract in the perpendicular direction of the applied force when subjected to a tensile strain. Zhang et al. [18] carefully examined this usual result by calculating the lateral response in the *y*-direction when a tensile strain is applied to the lattice in the *x*-direction. They found that the equilibrium lattice constant in the *y*-direction is expanded in all the cases of the strain applied to 7%, confirming the NPR of PG. This feature broadens plenty of its mechanical applications and also secures a prime position for PG in the class of nano-auxetic materials [62]. Unlike usual materials, the nanoscale auxetic materials become wider in the lateral directions (rather than shrink) under the application of uniaxial tensile strain [72,81,82]. Besides, these materials are rarely observed in nature but artificially characterized due to potential mechanical (enhanced shear resistance and fracture toughness, etc.) and technological applications [81,83,84]. Although an increasing awareness has been seen in recent years for exploiting the mechanical performance of 2D materials with in-plane and out-of-plane negative Poisson's effect, our intention is not to review all the literature that has been done on these materials; instead, we focus on PG and its mechanical potential that emerges from its in-plane auxeticity.

Based on extensive computational studies, two pioneering groups have parallelly reported the origins of NPR in PG. Initially, Zhang et al. [18] predicted that the in-plane auxeticity of PG mainly originates due to lattice interplay (Coulombic repulsion/bond rotation) between the sp^2 bonded carbon atoms. On the other hand, Sun et al. [28] utilized DFT and fourth-order continuum elastic theory to investigate nonlinear mechanical properties and the origin of NPR in PG [28] and introduced an atomic de-wrinkling mechanism for the auxetic behavior of PG under tensile deformation. Winczewski and Rybicki [62] also concluded that the de-wrinkling criterion can explain the auxeticity in PG. In a recent study, it was proposed that a negative Poisson's ratio may originate from three mechanisms: opening of the re-entrant units, rotation, and flattening effect [85]. For PG, it was identified in our previous study that the rotation of sp^2-hybridized C atoms induces its auxeticity (see Fig. S10 in Ref. [18]. However, despite such a vast expansion of knowledge, further studies are needed to prove the credibility of these results.

In addition, it was found that the in-plane auxeticity of PG can be tuned via surface defects and chemical functionalization. DFT calculations have shown that the vacancy defect concentrations of 3% and 6% and appropriate chemical functionalizations (hydrogenation and fluorination) convert NPR to positive values [71,86], and the NPR values are found to be > 0.235 for hydrogenated and fluorinated PG sheets [24]. On the basis of these findings, one can conclude the feasibility of PG in future mechanical applications.

Ultrahigh ideal strength

The ideal strength is one of the most prominent mechanical features that characterize the large-scale mechanical applications of 2D materials. From a theoretical point of view, it is defined as the highest possible strength offered by a nanomaterial in the absence of any topological defects under maximum stress conditions. Mechanically, the nanoscale behavior of 2D materials can be investigated by various fundamental factors such as in-plane stretching, compatibility against critical strain, and how it responds under the applied stress-strain situation. Besides the auxeticity at ambient conditions, PG is found highly stretchable under different stress-strain environments. Theoretically, an ultrahigh ideal strength of PG was observed by holding up the equibiaxial tensile strain of 17.1% [18], which is even higher than that of graphene (14.7%). While Kilic et al. [76] reported a maximum uniaxial strain of 17% and biaxial tensile strain of up to 21%, as shown in Fig. 3g. Numerically, DFT and MD calculations have witnessed a high ultimate tensile strength of 20 – 29.23 N/m in PG under uniaxial and biaxial tensile loading [18,28,61,74,87]. Furthermore, Zhang et al. [25] showed that chemical functionalization can effectively improve the stress-strain relationship of PG (Fig. 3h), and consequently, the ideal mechanical strength, in contrast to graphene, exhibits an insensitive mechanical response upon complete hydrogenation [88]. Excitingly, these emerging features not only uncover new mechanical aspects of PG but also could outperform the mechanical superiority of graphene [18,60].

Out-of-plane piezoelectricity

The study of piezoelectric effects in 2D materials provides more freedom in designing/synthesizing nanoscale devices with improved mechanical performance beyond our expectations. Generally, piezoelectricity refers to the ability of materials that can generate polarization charges/electrical potential in response to externally applied mechanical stress. Conversely, they could also experience mechanical stress/displacements under the effect of applied electric fields [89]. Piezoelectricity arises when a crystalline structure is both noncentrosymmetric and semiconducting, and the exact piezoelectric modes are determined by its space group symmetry. In this regard, literature surveys two kinds of piezoelectric materials based on their in-plane and out-of-plane piezoelectric responses under stress environments. Here, it is important to mention that the structural non-centrosymmetry is referred to as the main origin of the in-plane piezoelectricity [90–93], and notably, materials with in-plane effects have attracted significant interest due to their wide-ranging applications, e.g., actuators, energy harvesters, sensors, and Schottky barriers, etc. [94]. On the other hand, some materials with non-centrosymmetric structures also exhibit pure out-of-plane piezoelectric response under the effect of mechanical stress. In general, the out-of-plane piezoelectric coefficients of monolayer materials are relatively small, because such materials are very thin, and the spatial separation of positive and negative charges in their out-of-plane direction is limited. There are two main contributing factors to the out-of-plane piezoelectric effect: the hardness of a material (modulus of elasticity), and the magnitude of the electric dipole moment in the out-of-plane direction; the latter depends on the thickness and charge polarization. Although significant progress has been made in these materials due to their feasibility in bottom/top gate technologies [95], their topological rareness still demands more explorations in nature.

As a representative of the 2D class, the highly centrosymmetric nature and semimetallicity of graphene prevent it from being piezoelectric in its pristine format. In contrast, the prospect of piezoelectricity in PG is mainly adored to its semiconducting feature and intrinsically buckled atomic configuration; the latter induces non-centrosymmetricity in PG to generate an electric potential with a very active response upon applied stress. Additionally, there are two main strategies to enhance the out-of-plane piezoelectric coefficients of PG. One is surface functionalization as proposed by Wang's group [30], they introduced functional groups of hydrogen and

fluorine at the top- and bottom-layer of the PG sheet to modify piezoelectric response in the *z*-direction, and the other is introducing some other elements in PG to form binary compounds such as penta-CB_2 [80], and to form ternary penta-sheets [44,45,96]. Although the surface functionalization can improve the out-of-plane polarization, the resulting effect is not intrinsic for the penta-sheets, different from the intrinsic polarization induced by the polar bonds in the penta-sheets composed of multi-elements [44,45,96].

Guo et al. [80] theoretically tuned out-of-plane piezoelectricity in unstrained PG with the values of piezoelectric coefficients of $d_{36} = -0.065$ pm/V and $e_{36} = -0.099 \times 10^{-10}$ C/m, which are very small. Thus, they adopted two strategies, namely, strain-inducing and generating a Janus penta-monolayer by replacing the carbon atoms on the top atomic layer of PG with boron atoms, for enhancing the piezoelectricity. They found that the applied compressive strain (uniaxial and biaxial) can slightly improve the piezoelectric response of PG by 3.1% for 2% biaxial strain and 13.9% for 4% uniaxial strain, as depicted in Fig. 3i, while for the Janus penta-monolayer the out-of-plane piezoelectric response is obviously enhanced with much higher values of $d_{31} = -0.505$ pm/V and $d_{32} = 0.273$ pm/V, as compared to pristine PG and many other 2D materials [97,98]. A possible reason is that partially replacing C with B introduces a C—B polar bond, which increases the polarization of the system. With these studies, one can deal with various piezoelectric properties of such 2D materials for future piezoelectric applications.

Electronic properties

Geometrically assembled materials and their uniqueness in nature strongly depend on their underlying electronic structures and how they offer their electronically unique structure-property relationships. Especially for PG, extensive research has been done to probe its electronic properties by using various advanced theoretical approaches, including DFT, GW, and the tight binding. In this section, we review the progress made in the study of the electronic properties of PG, focusing on its band structure and carrier mobility.

Band structure from DFT

Theoretical prediction and nanoscale visualization of novel materials have generated a massive quantity of knowledge and widened scientists' vision towards materials discovery and computational simulations. Referring to mature theoretical approaches in computational materials physics and condensed matter physics, DFT has revolutionized modern sciences in exploring/tuning structural morphology and bonding chemistry of advanced materials and complex crystal structures. More specifically, assisted with the advancement of approximation functionals, e.g., local density approximation (LDA), generalized gradient approximation (GGA), and hybrid functionals to the exchange-correlation energy, modern DFT enables researchers to design novel materials with tailored properties and also set valuable criteria for their experimental realization under various environments.

The increasing research enthusiasm for PG is mainly driven by its intrinsic and highly tunable electronic band structure under various conditions. Compared to graphene, the emergence of electronic bandgap in PG is mainly due to the hybrid atomic configuration of C atoms. Recalling from Section *Geometry and stability of PG*, each C1 atom is in four-fold coordinated sp^3-hybridized bonding environments with four neighboring C2 atoms with three-fold coordinated sp^3-hybridization, suggesting the absence of any delocalized states in the whole structure. On the other hand, C2 atoms facilitate non-planar three-fold coordinated sp^2 configurations with one C2 and two C1 atoms, in which original π bonds between C2 atoms are formed by p_z electrons, and consequently, the bond length between C2 atoms is slightly reduced due to non-planarity, and p_z electrons become localized by leading to an intrinsic electronic bandgap in PG [26].

The band structure calculations at the GGA/PBE level imply that PG is an indirect bandgap semiconductor with a value of 2.20–2.42 eV [55,57,58,72,99–106]. The most striking feature of PG is its emergence as a quasi-direct bandgap semiconductor due to the existence of sub-valence band maxima (VBM) near the true—VBM region [18]. More interestingly, Shahrokhi [99] and Li et al. [100] have calculated the bandgap with the same value of 2.22 eV (at the PBE level) for the indirect/direct band structures in two different studies. Unlike 2D hexagonal sheets, such as graphene, graphyne, and graphdiyne, there is no need to functionalize PG for opening band gap. This factor renders PG as a more versatile material in semiconductor and photocatalytic science and could provide new opportunities for the development of optoelectrical and electronic devices.

On the other side, it is well known that the derivative discontinuity of exact exchange-correlation energy in semi-local DFT functionals (e.g., LDA, GGA) underestimates the intrinsic bandgap of the semiconductors [63,107,108] and strongly demands more accurate functionals. This concern has motivated the development of non-local hybrid functionals, e.g., Heyd-Scuseria-Ernzerhof (HSE06) functional, which include both DFT and Hartree contributions to estimate the intrinsic electronic bandgap of nanomaterials with high accuracy [109]. More interestingly, the HSE06 functional retains indirect to quasi-direct band structure in PG (Fig. 4a) by improving its bandgap from 2.20 eV (PBE) [58] up to 3.25 eV [18] and 3.44 eV (HSE06) [100]. Furthermore, the density of states (DOS) of PG in Fig. 4a manifests that the valence and conduction bands near the Fermi level of PG are mainly dominated by sp^2-type energy states. However, benefitting from PG's indirect to quasi direct bandgap character, scientists anticipate even a larger bandgap for PG on experimental grounds due to the limiting behavior of DFT simulations. In this respect, significant attention is paid to bandgap engineering in PG through various tuning strategies, such as heteroatoms doping, chemical functionalization, strain configuration, etc., to extend its electronic performance in multiple directions.

Integration of chemical dopants into a pure lattice preferentially demands physical and electronic similarity with subjected lattice at ambient conditions. In this regard, previous literature has shown that the inclusion doping of heteroatoms (B, N, and P, etc.) can facilitate dramatic changes in structural and physical properties of the carbon family by maintaining structural symmetry unchanged [103,110–114]. As a derivative of this family, these substitutions also have been utilized in PG to exploit its electronic performance and potential uses in optoelectrical applications. For example, Berdiyorov et al. [55] patterned substitutional dopings of Si, B, and N atoms in PG sheet and observed a bandgap reduction of ~ 0.2 eV, although the reducing magnitude strongly depends on the location and type of dopant atoms. In this vein, many other DFT studies have also reported the bandgap reduction in PG after the doping of substitutional atoms at different locations [34,69,106,115].

Besides the doping strategies, chemical functionalization is also an effective technique to regulate the bandgap of PG. Li et al. [24] showed that chemical functionalization (hydrogenation and fluorination) widens the bandgap of PG and specifically converts its semiconducting nature closer to the insulators. Liu et al. [116] reported that hydrogen adsorption on the PG sheet can lead to a transition from semiconductor to half-metal by modifying the electronic properties of the functionalized PG. By applying the HSE06 functional, Jia et al. [30] reported bandgap extension in PG from 3.25 eV to 4.42, 4.61, and 4.86 eV after fluorination, hydrofluorination, and hydrogenation of PG sheet. In addition, Li et al. [100] also have analyzed bandgap widening for oxygenated PG sheet due to the rigid-up-shifting of the conduction band under increasing coverage of oxygen.

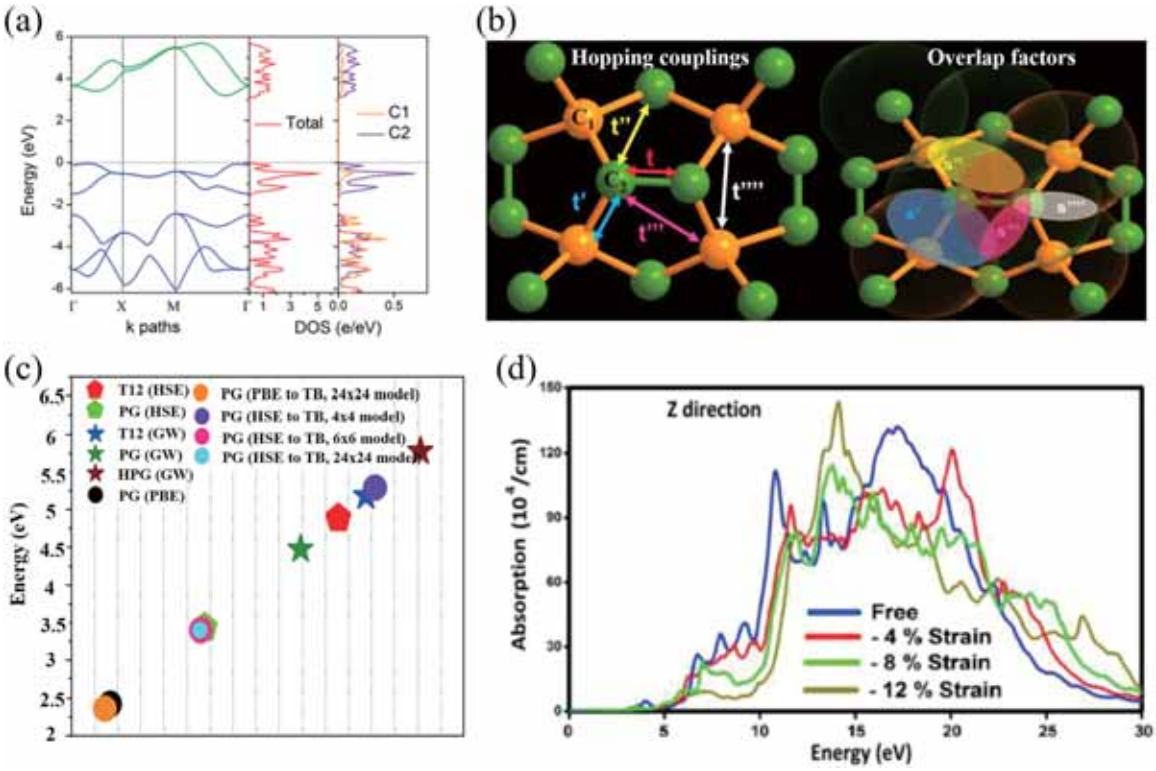

Fig. 4. (a) Calculated electronic bandgap of PG and corresponding DOS at the HSE06 level. (b) Illustration of TB parameterized hopping energies and overlap factors between the C atoms of PG. (c) Calculated bandgap values (taken from Table 2) of T12 carbon, PG, and H-PG by using DFT at the PBE and HSE06 levels and GW and TB methods. (d) Strain-modulated absorption spectra of PG. The colorful lines indicate compressive strain coverages from 0% to 12%, respectively.
(a) Adapted with permission from Ref. [18]. Copyright 2015, National Academy of Science. (b) Adapted with permission from Ref. [117]. Copyright 2020, IOP Publishing. (d) Adapted with permission from Ref. [102]. Copyright 2019, Elsevier.

In addition to doping and chemical modulations, the external strain also plays a vital role in tuning the bandgap of PG. Yu and Zhang [23] showed about 4.18% bandgap reduction in PG by applying biaxially strained effects. Using the HSE06 functional, the authors calculated bandgap values of 3.29 and 3.13 eV by applying −3% compressive and +3% tensile strain configurations. Shahrokhi [99] suggested that biaxially applied tensile strain increases the band gap, whereas compressive strain considerably decreases the bandgap values of PG. In accordance, Alborznia et al. [102] showed that vertical compressive strain moderately reduces the electronic bandgap of PG from 2.23 eV to 1.25 eV (at the PBE level) and notably drives indirect to direct bandgap transition in PG.

Band structure from GW

It is well-known that DFT calculation underestimates bandgap. To relieve this concern, one of the possible and highly efficient formulism is using ab initio GW approximation ($\sum = \iota GW$), which investigates the electronic band structures of materials by considering self-energy operator ($\sum$) of single-particle (electron), Green function (G), and screened Coulomb interaction (W). Usually, the GW approach results in larger bandgaps close to the experimental values by correcting the many-body effects compared to DFT calculations. In the case of PG, Einollahzadeh et al. [26] studied that the single-shot GW approach (G_0W_0, known as the first-order correction to single-particle Hamiltonian) could improve the bandgap of PG by up to 2 eV and computed a quasi-direct bandgap of 4.1–4.3 eV. Shortly after, Wang et al. [29] validated this study and calculated the bandgap value of 4.48 eV for pristine PG and 5.78 eV for hydrogenated PG by employing the G_0W_0 approximation. From these findings, it is worth noting that the GW approach characterizes PG as a wide band gap semiconductor with potential applications in electronic devices.

Band structure from tight binding

Although DFT and GW formalisms effectively regulate the electronic band structure of PG, the difference between the calculated values cannot be ignored. In addition, they also demand advanced computational functionalities in case of the increasing number of atoms in the unit cell, which could increase calculation costs and time intervals. At the same time, the tight-binding (TB) approach exhilaratingly relieves the cost concerns and efficiently provides an adequate and accurate analytical description of the electronic band structure.

Based on the TB approximation, several studies have investigated the electronic band structure of PG via suitable parameterizations such as the Slater-Koster approach, four-band model, hopping parameters, overlap factors, and onsite energies, etc. [27,59,117]. Fig. 4b shows the interactions of hopping couplings (t', t'', t''', and t'''') and overlap factors (s', s'', s''', s'''') between C1 and C2 atoms in PG [117]. From Fig. 4b, it is worthy to note that the energy-dependent hopping elements can reproduce the characteristics of DFT bands and also elaborate the two highest valence and lowest conduction bands within the four band model [27]. Interestingly, it is found that the inclusion of the onsite energies adequately approximates the parameters of the four-band model [27], whereas overlap factors locate and identify the position and shape of the conduction bands [117]. Besides, the application of a vertical electric field reduces the bandgap of PG in the TB model [117]. In order to compare the performance of TB parameters, the computed maximum bandgaps of PG by employing DFT, GW, and TB methods are summarized in Table 2 and presented in Fig. 4c.

Ultrahigh carrier mobility

Carrier mobility is one of the most crucial factors of nanomaterials for estimating their conductive performance in advanced

Table 2
Bandgap values (in eV) of PG obtained from DFT at the PBE and HSE06 levels, GW, and TB methods. For comparison, the results for T12 carbon and H-PG are also listed here.

System	Methods				
	PBE	HSE06	GW	PBE to TB	HSE06 to TB
T12		4.89 [29]	5.19 [29]		
PG	2.20 [58]	3.22 [106]	4.1–4.3 [26]	2.19–2.36 [59]	3.25–3.40 [117]
	2.21 [57,72]	3.24 [101]	4.48 [29]		3.25–5.29 [27]
	2.22 [99,100]	3.25 [55]			
	2.23 [101,102]	3.26 [76]			
	2.26 [118]	3.27 [29]			
	2.27 [55]	3.29 [119]			
	2.29 [104]	3.44 [100]			
	2.31 [102]				
	2.40 [105]				
	2.42 [106]				
H-PG			5.78 [29,107]		

electronics and photocatalytic applications. Particularly, the carrier mobility (μ) of 2D materials is mainly governed by three parameters: elastic modulus, effective mass, and deformation potential constant [120], and can be calculated by using the following formula [120–123],

$$\mu_{2D} = \frac{e\hbar^3 C_{2D}}{k_B T m_e^* m_a E_1^2} \quad (1)$$

where e is the electronic charge, $\hbar$ is the reduced Planck's constant, C_{2D} is the elastic modulus of longitudinal strain along the transport direction of 2D materials, k_B is Boltzmann constant, T is the room temperature, m_e^* is the effective mass of the charge carrier (electron/hole) along the transport direction, m_a is the average effective mass, and E_1 is the deformation potential constant. Specifically, the carrier mobility in 2D materials is mainly governed by three parameters: elastic modulus, effective mass, and deformation potential constant [120].

The large electronic bandgap and considerable separations between the charge carriers have produced a significant interest in exploring the carrier mobility of PG. In the light of this consideration, Deb et al. [118] systematically investigated the ultrahigh charge-carrier mobility of PG and numerically found it to be 22.74×10^3 cm^2/Vs (electrons) and 1.27×10^3 cm^2/Vs (holes) at room conditions, and 11.72–40.9 $\times 10^3$ cm^2/Vs (electrons) and 0.66–1.51 $\times 10^3$ cm^2/Vs (holes) for strained conditions. Notably, the fine-tuned carrier mobility of PG is mainly credited to higher elastic constant and lower effective masses of the charge carriers [118]. In addition, chemical doping also offers a positive impact on the carrier mobility of PG. According to Guo et al. [80], the electron mobility of B-substituted PG can reach up to a high magnitude of 8.87×10^3 cm^2/Vs along the y-direction. As compared to many 2D materials [124–127], the ultrahigh carrier mobility of PG could offer potential edges in electronic devices such as logic circuits and field-effect transistors (FETs).

Optical properties

As a consequence of the highly tunable electronic band structure, PG has drawn considerable attention in its optoelectrical applications. Interestingly, DFT calculations have revealed that PG covers a wide range of optical absorption from visible to ultraviolet (UV) regions [29,106]. However, according to Einollahzadeh et al. [26], the GW approach characterizes PG as a wide bandgap semiconductor that limits the direct emergence of photoelectrons by making it transparent in the visible light spectrum. As discussed in the above sections, PG has a strong ability to respond the external stimuli such as substitutional dopings, chemical functionalization, and external strain in a controlled manner. In the light of this motivation, Dai et al. [106] reported that substitutional dopants (Al, Si, P) narrow the effective width of the absorption spectrum of PG and also shift the absorption edges toward the redshift regions. Stauber et al. [27] determined the isotropic absorption of PG up to 24% by applying TB parameterization. Wang et al. [29] have disclosed that hydrogenation extends the optical absorption of PG by increasing the optical bands at the conduction band edges. Shahrokhi [99] systematically investigated external strain impacts (including tensile strain and compressive strain) on the optical properties of PG. They concluded that increasing the magnitude of compressive strain can convert the absorption edges, optical conductivity, and electronic energy loss to the redshift (lower energy) regions, whereas tensile strain, in contrast, can shift them to blue shift (higher energy) regions [99]. In a similar trend, Alborznia et al. [102] also showed reduced absorption of PG by applying the compressive strain of 0–12% (Fig. 4d). From these findings, it can be concluded that these tunable strategies not only probe the optical response of PG but could also bring new opportunities in designing PG-based optoelectrical devices.

Thermal transport and thermoelectric properties

The lattice thermal conductivity of carbon materials is of great interest, as it varies in a wide range, from 0.01 W/mK (amorphous carbon) to over 3000 W/mK (diamond), depending on their crystal structures. Graphene has an ultra-high thermal conductivity of 3000–5300 W/mK at room temperature [128–130]; it would be interesting to know that how high the corresponding value for PG is and how sensitive the thermal conductivity is to defect, grain boundary, strain, and surface modification as PG has a completely different crystal structure from graphene. In this light, this section presents a summary of PG's thermal properties, which would promote it as a future thermal material for potential applications in thermal science and management.

Intrinsic lattice thermal conductivity of PG

Lattice thermal conductivity ($\kappa_{lattice}$) refers to the ability of a lattice to dissipate/conduct heat by controlling the working temperature. The thermal conductivity in metals is mainly credited to electrons, while in non-metals (e.g., semiconductors and insulators), it is carried out by lattice vibrations (phonons) due to the absence of high-density free electrons [128].

Considering the unique morphology and semiconducting feature of PG, a great deal of attention has been paid to exploring its lattice thermal conductivity under different conditions. Boltzmann transport equation, DFT, and potential-based MD simulations have been employed to investigate the intrinsic thermal conductivity of PG. Xu et al. [31] explored the temperature-dependent thermal response of PG and revealed an inverse relationship between the thermal conductivity and applied temperature. They obtained the value of 167 W/mK as the intrinsic lattice thermal conductivity for PG at room temperature by utilizing the original Tersoff interatomic potential (MD simulations), which is the best and most suitable atomic potential to describe the PG model, according to Winczewski [60]. Furthermore, they also concluded that up to 90% of thermal conduction in PG is mainly dominated by acoustic phononic branches and phonons with the mean free paths larger than 100 nm. By employing other various potentials, PG's thermal conductivity is calculated to be 112.35 W/mK (ReaxFF potential) [131], 197.85 W/mK (BTE) [132], 392 W/mK (Tersoff potential) [133], and 518 W/mK (DFT-D vdW functional) [134], respectively. In a similar vein, Wang et al. [32] predicted a more prominent value of 645 W/mK by solving the phonon Boltzmann transport equation and combining it with DFT

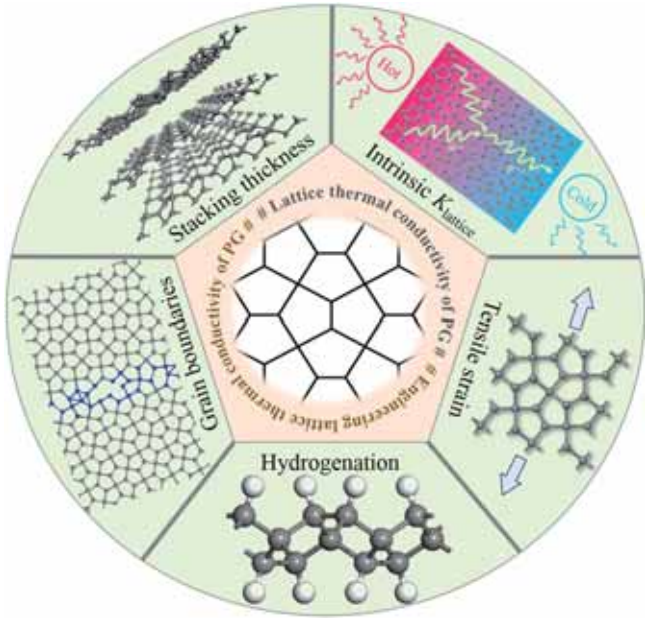

Fig. 5. An overview of thermal engineering of PG by employing stacking, grain boundaries, hydrogenation, and tensile strain.

calculations (Fig. 6a). Compared to graphene, the much lower intrinsic lattice thermal conductivity of PG is attributed to various factors such as strong anharmonic scattering in PG induced by the hybrid sp^2 and sp^3 bonding nature and its buckled atomic configuration and the applied simulation method and potential [32,135]. Aiming at improving performance, several tuning strategies such as stacking mechanism, grain boundaries engineering, chemical functionalization, and mechanical strain have been applied to regulate the intrinsic thermal conductivity of PG (Fig. 5). These factors can not only effectively turn the thermal conductivity of PG but also provide new opportunities for this material.

To study the dependence of the lattice thermal conductivity of PG on its stacking thickness, Wang et al. [136] explored the thermal response of the stacked PG and found that, unlike graphene, the thermal conductivity of the stacked PG is insensitive to the number of layers, as shown in Fig. 6b. Because the interlayer-interaction in stacked PG is van der Waals interaction which is very weak, hardly has many effects on the thermal conductivity, and the buckled structure lacks the reflection symmetry and breaks the 2D selection criteria for three-phonon scattering.

On the other hand, the thermal conductivity of PG can also be tuned via grain boundaries (GBs) engineering. At room conditions, Sun et al. [137] investigated the effect of grain boundaries on the thermal conductivity of PG by employing non-equilibrium (NEMD) simulations. They reported that the existence of GBs can decrease the thermal conductivity by about 20% in polycrystalline PG due to the geometric anisotropy, low phonon group velocity, and strong phonon scattering induced by GBs. In addition, the boundary conductance of polycrystalline PG, compared to pristine PG, can be modulated to the lower ranges with different grain orientation angles [137].

Chemical functionalization is also an important and reliable approach to tune the thermal conductivity of PG. By combining DFT and BTE, Wu et al. [138] showed that full hydrogenation (100% coverage) dramatically improves the thermal conductivity of PG, up to 76% (Fig. 6c), as compared to the pristine PG. This enhancement is mainly attributed to weakened bond anharmonicity and elimination of asymmetric π-bonds between the C atoms in sp^2-hybridizations in PG after hydrogenation [138] and fluorination. While Zhang et al. [131] performed NEMD simulations and found that the thermal conductivity of PG increases when hydrogenation coverage is less than 25% but decreases for higher coverage. Furthermore, they found that the decoration of hydrogen and oxygen atoms on the outer layers of PG leads to a down-and-up oscillation in thermal efficiency

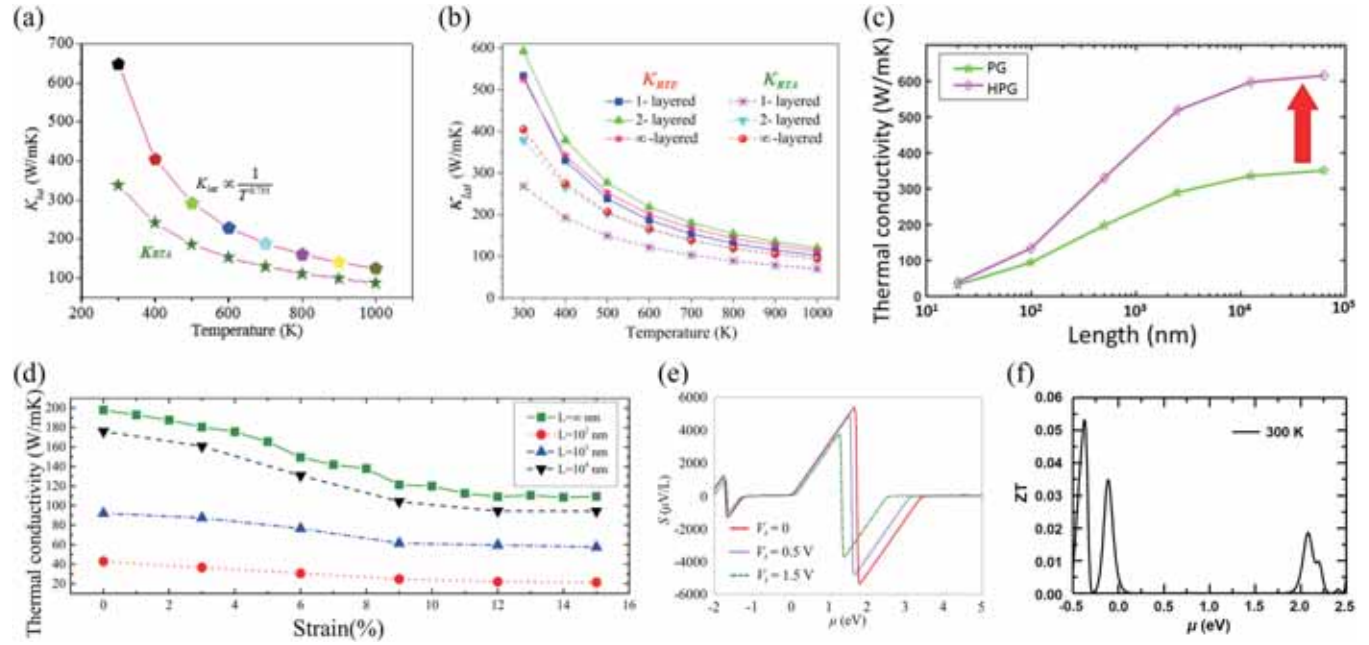

Fig. 6. (a) Temperature-dependent intrinsic thermal conductivity of PG, (b) Layer-dependent thermal conductivity of stacked PG, calculated by linearized BTE and relaxation time approximation (RTA) solutions, (c) Thermal conductivity of PG and hydrogenated PG (HPG) as a function of increasing length, (d) Strain-modulated intrinsic thermal conductivity of PG at different system sizes (L), (e) Theoretically calculated Seebeck coefficient of PG for different gate potentials at room temperature, (f) Theoretically predicted *ZT* value of PG at 300 K.

(a) Adapted with permission from Ref. [32]. Copyright 2016, Elsevier. (b) Adapted with permission from Ref. [136]. Copyright 2017, American Institute of Physics. (c) Adapted with permission from Ref. [138]. Copyright 2016, American Chemical Society. (d) Adapted with permission from Ref. [132]. Copyright 2016, American Chemical Society. (e) Adapted with permission from Ref. [117]. Copyright 2020, IOP Publishing. (f) Adapted with permission from Ref. [57]. Copyright 2017, IOP Publishing.

in PG, and a fully decorated PG sheet exhibits almost the same thermal response as a pure PG. To solve these inconsistent results, more in-depth studies, such as including four-phonon-scattering in DFT and carefully checking the validation of the atomic potential in MD simulations, are needed.

In addition to surface functionalization, a significant reduction in the thermal conductivity of PG is observed in its tensile strain configuration. Liu et al. [132] analyzed an obvious reduction of 41% in the lattice thermal conductivity of PG when a tensile loading of 11% was applied (Fig. 6d). More interestingly, it was also reported for graphene that even an 8% tensile loading reduces its thermal conductivity by up to 42% [139]. From these findings, it can be inferred that the thermal response of PG behaves likely to that of graphene under tensile strain.

Thermoelectric efficiency of PG

The intrinsic thermal conductivity of PG is found to be ~10–15% of the value of graphene [128–130], showing much potential for thermoelectric applications [140–142]. The thermoelectric efficiency of materials can be estimated by the dimensionless figure of merit ($ZT = S^2\sigma T/\kappa$), where S, σ, T, and κ are Seebeck coefficient, electronic conductivity, temperature, and the total thermal conductivity (mainly contributed by both: electrons and phonons) [143]. In this favor, theoretical calculations have witnessed that the Seebeck coefficient and the value of ZT of PG are 36–67 times greater and about six times higher than those of pristine graphene, respectively (Fig. 6e-f) [57,117]. This encouraging thermoelectric performance of PG mainly originates from its intrinsic and tunable electronic bandgap, lower thermal conductivity, and high Seebeck coefficient. In addition, the larger relaxation time of holes makes PG a better *p*-type thermoelectric material at room conditions [57]. Furthermore, Chen et al. [57] also predicted that the application of tensile strain can effectively tune the value of ZT as well as *n*-type and *p*-type power factors ($P = S^2\sigma$) of PG. They found that PG's power factor and *p*-type ZT values can be enhanced up to 16.1 and 9.1 times by imposing a tensile strain loading of 11%.

Adsorption properties

The accelerating depletion of sustainable energy sources and the worsening of environmental degradation caused by the rapid consumption of fossil fuels have inspired modern societies to develop highly efficient, versatile, and ecofriendly energy sources/storage systems and their proper utilization. In this regard, dimensionally confined carbon-based adsorbents have attracted significant attention as cost-effective, highly efficient, and portable energy sources due to their large surface area and tunable adsorption/desorption properties. PG is an emerging example in this class because its highly remarkable/tunable optoelectronic properties have prompted significant research enthusiasm to explore its adsorption and storage properties [144–146]. In addition, the fused sp^2 C atoms in the PG sheet induce more chemically active sites, which offer a predominant role in the adsorption/desorption of gas molecules at ambient conditions. Following these considerations, this section discusses the research advances of PG as an energy storage candidate.

CO_2 capture and storage

The increasing emission of carbon dioxide (CO_2) with the current level of ~ 414 ppm (till date) in the atmosphere [147] has produced alarming concerns regarding global warming and environmental problems such as the greenhouse effect, raised sea level, climate change crisis, etc. Therefore, it is highly imperative to tackle these prevailing issues by minimizing CO_2 emissions across the globe. In the case of adsorbents for CO_2, carbon materials have won considerable attention due to their chemical flexibility and abundance in nature. Furthermore, their adsorption behavior can be regulated by altering their morphology, chemical composition, and surface environments under room conditions. In the light of these motivations, Wang et al. [148] explored the electric field-controlled adsorption behavior of PG by varying the electric field conditions from 0.005 to 0.040 a.u. They noticed the transformation of physisorbed CO_2 molecule to chemisorbed one by applying an electric field ranging of 0.025–0.030 a.u. and controlled CO_2 capture/release between the value of 0.030–0.040 a.u. Furthermore, they revealed remarkable adsorption with enhanced binding strength of CO_2 molecules on the PG sheet under the effect of an external electric field. In order to extend the adsorption strength of CO_2 molecules on the PG sheet, metal atoms doping has also been utilized in several reports. For example, Zhang et al. [149] found that the doping of Fe atoms induces a chemical bonding environment between CO_2 molecules and sp^2 C sites and thus strengthens CO_2 adsorption on different sites in PG. Sathishkumar et al. [150] extended this concept to charged and electric field-controlled CO_2 capture on N-doped PG sheet. They found that doping of N atoms efficiently raises the adsorption/desorption of CO_2 on PG, and this process can be reversed and controlled by switching (on/off) charged states and applied electric field. More importantly, it is worthy to note that the weak adsorption of other species such as H_2, CH_4, and N_2 is found on PG, which promotes the controlled separation of CO_2 from the PG sheet [148–151]. These outcomes clearly indicate that PG not only has huge potential as a CO_2 adsorbent but also proves its superiority as a highly efficient, controllable CO_2 capture and separation under different external environments.

Adsorption of DNA/RNA species

The progressive development of graphene and its structural analogs have inspired a strong interest in sensing devices to relieve the complexity of medical and biological treatments. Fortunately, their ultrathin morphology, large surface-to-volume ratio, and high sensitivity of active sites provide maximum interaction response with adsorbed molecules for molecular and bio-sensing applications. Compared to other 2D materials, the most striking features of PG are its unique geometric and electronic structure that make PG as an interesting platform to explore the behaviors of adsorbing deoxyribonucleic acid (DNA) and ribonucleic acid (RNA). Recently, Li and Shao [70] employed DFT calculations to investigate the adsorption behavior of deoxyribonucleic/ribonucleic acid (DNA/RNA) elements, including adenine (A), cytosine (C), guanine (G), thymine (T), and uracil (U), and three base pairs GC, AT, and AU on PG sheet. They examined strong adsorption of nucleobases and base pairs on the PG sheet with binding energies of – [0.50–1.10] and – [1.40–1.70] eV, respectively. The adsorption strength follows the order of G > A > C > T > U and GC > AT > AU. Furthermore, they also found the enhanced stability of (8–44%) of these DNA/RNA elements on the PG sheet, which firmly shows the potential of PG for biosensing applications.

Hydrogen storage

For the economic development of hydrogen storage materials, previous literature has shown that carbon materials provide an intriguing environment for the adsorption and desorption of hydrogen molecules at ambient conditions [152–160]. Equally important, as discussed before that PG also offers intriguing sorbent conditions due to its unique geometry and bonding feature. Considering this motivation, multiple studies have investigated the capability of PG for hydrogen storage. For instance, by combining DFT and Monte Carlo (MC) simulations, Enriquez and Villagracia [34] showed that the substitutional doping of 3*d* transition metals (TMs) enhances the capacity of PG sheet for non-dissociative H_2 storage with the adsorption energy of E_{ads} = 0.092 eV as compared to that of graphene with E_{ads} = 0.067 eV. Following this idea, bimetallic particles and

clusters have also been used to increase hydrogen storage efficiency on PG sheets [161,162]. In addition to the decoration of TMs, Sathishkumar et al. [115] found that doping heteroatoms (B and N) can effectively promote PG's potential for hydrogen storage. They further suggested that the doped PG decomposes H_2 molecules into H atoms with strong adsorption energy. Furthermore, increasing the concentration of dopant atoms can reduce the activation energy for H_2 dissociation.

Catalytic properties

2D materials with a high surface ratio have the potential as catalysts for oxygen reduction reaction (ORR), CO_2 activation, water-splitting, and carbon monoxide (CO) oxidation reactions [163]. The advantages of 2D carbon-based catalysts mainly arise from their ultralow weight, large surface area, and atomically thin nature, which prominently expose catalytically active sites and provide a favorable environment for these reactions under and beyond ambient conditions. Motivated by the unique geometrical configuration and the theoretically well-defined novel properties of PG, many efforts have been paid to study its catalytic activity under various conditions. This section firstly reviews the theoretical performance of pristine PG as a catalyst and then as a doped catalytic material.

PG as a metal-free catalyst for CO oxidation

Metal-free catalysts have emerged as important alternatives to metallic catalysts in the past few years. The precious metal-based catalysts (i.e., Au, Pt, Pd, Rh, and their alloys) have been served as CO catalysis since a long time ago, but a high temperature (> 100 ^oC) is usually needed to initiate the catalytic reaction. Moreover, the limited earth reserves and high reaction costs further restrict their catalytic applications in modern scientific areas. To relieve these catalytic limitations, there are increasing need for more green catalysts without metals.

Apart from the conventional 2D sheets, PG has also attracted widespread interest for its effectiveness in CO catalytic reactions. The catalytic fascination of PG mainly originates from its special geometry. In this light, Krishnan et al. [33] theoretically explored the catalytic efficiency of PG at low-temperature intervals by utilizing two well-established mechanisms, namely Eley-Rideal (ER) and Langmuir-Hinshelwood (LH). In the ER mechanism, the CO molecule directly interacts with an adsorbed O_2 molecule to develop a CO_2 molecule on the PG sheet. On the other hand, the CO and O_2 molecules are co-adsorbed on the PG sheet before the final interaction in the LH mechanism. The energy barriers for ER and LH mechanisms were calculated to be 0.65 eV and 0.31 eV [33], which are comparable to earlier reported metal-based catalysts [164,165]. In addition, the authors found that the PG sheet removes the generated CO_2 molecules due to lower adsorption energy in both mechanisms and recovers its original condition for the next oxidation cycles [33]. This factor promotes PG's catalytic performance in fuel cells to drive the low-temperature catalytic reactions, and also proves the novelty of PG sheet as a recyclable metal-free catalyst that can partially overcome some drawbacks of metal catalysts.

Catalytic performance under doping environments

The small fraction of dopants can regulate pristine lattice in the desired format and facilitate dramatic changes in the physical and electronic properties of 2D materials. These structural/electronic modulations usually promote the corresponding catalytic activity; however, their performance strongly depends on the doping concentrations. In the case of PG, the sp^2 atoms provide a suitable environment for catalytically active sites and promote the direct identification of single/hetero dopant atoms, resulting in an enhanced structural performance under doping environments. It has been discussed that heteroatoms doping (e.g., B and N) is an effective and reliable technique for modulating structural as well as electronic properties of PG.

Based on these considerations, Chen's group has done several works to investigate the effect of heteroatoms (B, N, and BN co-doping) doping on the catalytic performance of PG [166,167]. For example, they revealed that the substitution of the sp^2 C atoms with B and N atoms leads to polarization in PG due to considerable differences between electronegativities of host C and dopant atoms. Although these dopants reduce the intrinsic bandgap of PG, thereby producing strong interaction between overlapping electronic states of C and dopant atoms. Consequently, the modulation of electronic states dramatically improves the catalytic efficiency of PG. Such improvement was mainly observed in N-doped PG because of the higher electronegativity of N as compared to C atoms [166]. In addition, the B and N co-doping also enhances the catalytic efficiency of the PG sheet due to the lower reaction energy barriers [167]. Apart from heteroatoms doping, single-atom doping is also a promising strategy for tuning PG's electronic states and catalytic properties. In this regard, several groups have theoretically shown that Fe- and Pt-doped PG sheets can be served as single-atom catalysts (SACs) [168,169]. These atoms tend to hold on to the catalytically active sites of PG and improve its catalytic efficiency by maintaining overall symmetry at the same time. Benefitting from the above discussions, it can be concluded that PG has permissible potential for low-cost and eco-friendly CO oxidation and can initiate an appealing platform for low-temperature and metal-free catalytic reactions in its pristine or doped format.

Potential device applications

To meet the ever-increasing need for advanced multifunctional devices, scientists from several disciplines have collaborated to develop innovative materials, advanced integration procedures, and device architectural designs. Especially, 2D materials are of special interest for this topic. This section discusses the device applications of PG in heterojunctions, battery anode, and gas sensing.

Heterojunctions

While 2D materials exhibit many exciting properties that make them potential candidates for future electronics and multifunctional devices, combining these materials in the heterostructure form can enable coupled or enhanced properties, which are lacking for individual materials. A notable amount of research has been dedicated to designing both lateral and vertical vdW heterostructures, especially for graphene, boron-nitrides (BN), phosphorene, and chalcogenides [170]. For device applications, Guo et al. [36] and Zhao et al. [171] respectively reported a vdW heterojunction formed by vertically stacking graphene and penta-BN_2 on the PG sheet through state-of-the-art calculations (Fig. 7). Penta-BN_2 is slightly buckled as compared to PG, with a sheet thickness of 1.26 Å and metallic in nature [172]. When constructing a heterostructure based on two sheets, it is needed to find a commensurate lattice that can host supercells of both sheets and stack the two sheets in such lattice. However, the lattice mismatch between two different sheets is inevitable. The authors used their in-house code [36] to find out the commensurate lattices with a low lattice mismatch threshold of 2% to ensure that the internal strain is negligible, and with a constraint of the total number of atoms in the supercell less than 300 for the convenience of calculation. The basic idea is that, for a given interface area, all the possible supercells of the two sheets are generated and compared for the best match.

The electronic properties of both the PG/ graphene and PG/ Penta-BN_2 heterojunctions were preserved (Fig. 7d, g), forming vdW heterostructures. The Schottky barrier was evaluated by using the Schottky Mott rule. Both the heterojunctions form an *n*-type contact at the vertical interface and a negative band bending occurred by the

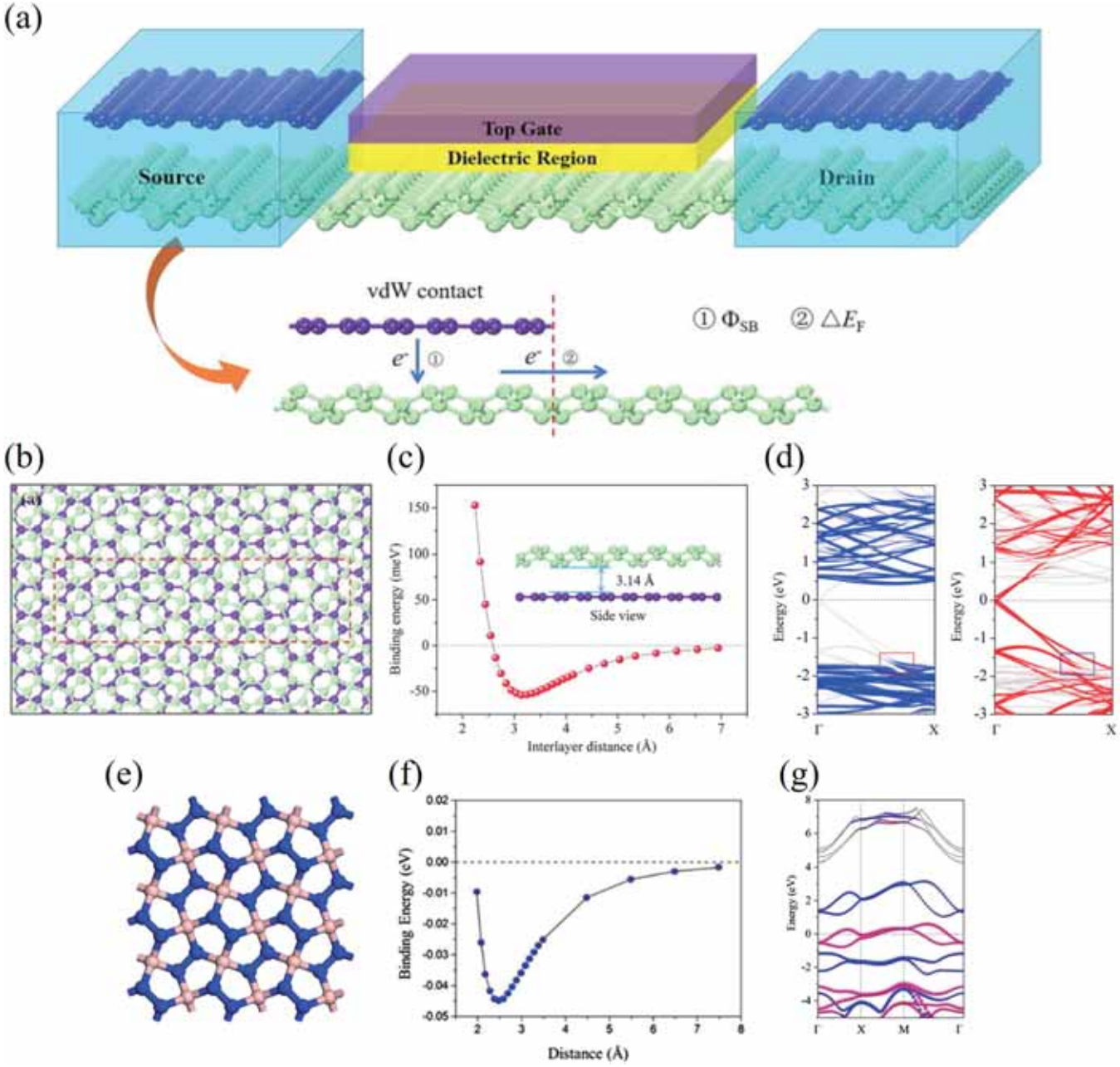

Fig. 7. (a) Schematic diagram of PG/graphene heterojunction-based transistor. (b) Top view of PG/graphene heterojunction. (c) Binding energy as a function of the interlayer distance between PG and graphene. (d) Projected electronic band structures of PG and graphene in PG/graphene heterojunction at the PBE level. (e) Top view of the free-standing penta-BN_2 sheet. (f) Binding energy as a function of the interlayer distance between PG and penta-BN_2.(g) Electronic band structure of PG/BN_2 heterojunction at the PBE level (the red and blue color lines show the contribution from penta-BN_2 and PG, respectively).
(a–d) Adapted with permission from Ref. [36]. Copyright 2017, American Institute of Physics. (e) Adapted from Ref. [172]. (f, g) Adapted with permission from Ref. [171]. Copyright 2018, AIP Publishing.

current in plane (CIP) device model at the lateral interface. Moreover, near Ohmic contact has been achieved in PG/graphene heterojunction with graphene as the metal electrode by applying an external electric field or doping with N atoms [36]. While for penta-BN_2/PG contact, although an Ohmic contact cannot be achieved, the Schottky barrier height can be modulated by applying stress and strain [171].

Chen et al. [173] systematically explored the interface interactions in an all-carbon heterostructure of PG and fullerenes (C_{20} and C_{60}) (Fig. 8a). PG forms a vdW type contact with C_{20} where only two C—C bonds can be formed between the heterojunction, whereas a covalent type contact is formed with C_{60} where two or four C—C bonds can be formed between the heterojunction. The electronic band gap of the PG/C_{20}(C_{60}) heterostructure is reduced as compared to that of PG because of the introduced electronic states from C_{20} and C_{60} near the Fermi level (Fig. 8b), thus making these systems suitable for visible solar light absorption [173].

Recently Yi et al. [174] theoretically proposed a lateral heterojunction composed of PG nanoribbon and penta-B_2N_4 nanoribbon, as shown in Fig. 8c, and studied its electronic and spin-dependent transport characteristics considering the cases of bare H and Cl atoms passivation. They found that under the positive biased voltage range between 0.7 and 1.3 eV, the heterojunction reaches a maximum value of spin-up current of 3.43 μA and decreases to a minimum value at 1.6 V, and then increases again with the increasing value of biased voltage. Similar behavior is observed under

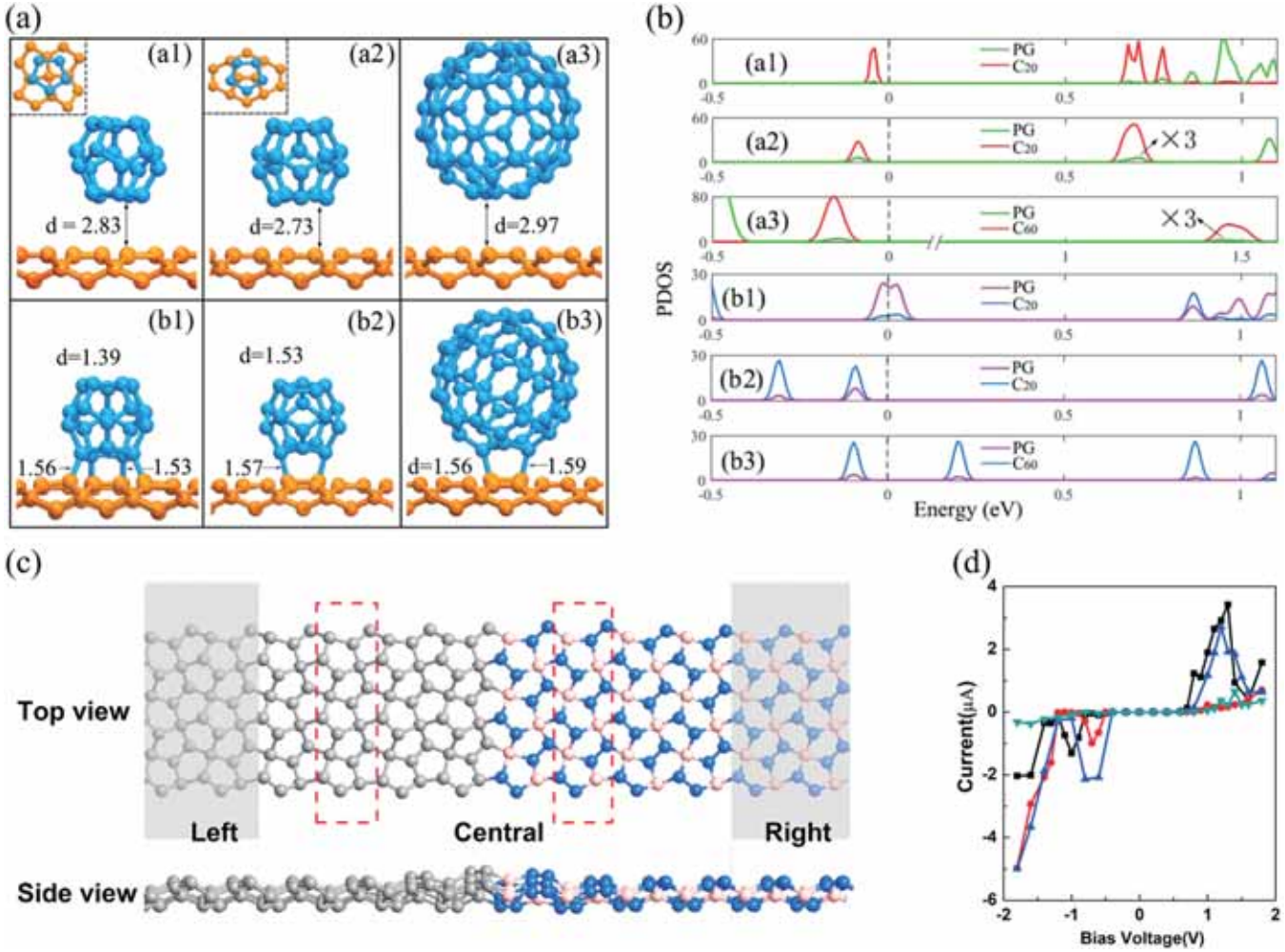

Fig. 8. (a) Side views of the geometries, and (b) the partial-DOS of the PG/C_{20}(C_{60}) heterojunctions. (c) Top and side views of the lateral heterojunction model, and (d) spin-dependent current-voltage curves of PG/penta-B_2N_4.
(a, b) Adapted with permission from Ref. [173]. Copyright 2018, IOP Publishing. (c, d) Adapted with permission from Ref. [175]. Copyright 2020, Elsevier.

negative biased voltage (Fig. 8d), thus showing a negative differential resistance under both cases. Spin filtering and spin splitting effects are also observed in the heterojunction with bare edges. Moreover, In the case of H passivation, the heterojunction has unidirectional conductivity, and for Cl passivation, the author reported a bipolar spin filtering effect [174].

On the other hand, in a real device, such as a field-effect transistor, contact between the channel material and metal is usually required to inject an appropriate type of carrier into the conduction or valance bands of the semiconducting channel. However, the biggest challenge that masks the intrinsic properties of the semiconductor is the lack of a low resistance metal contact. Hassan et al. [176] studied the physics underlying the contacts of PG with pure 2D metal electrodes covering a wide range of work functions. They found that PG undergoes metallization under all chosen metal contacts, as shown in Fig. 9 for an example of PG/Au contact. The theoretical study suggests that PG forms an *n*-type Schottky barrier when in contact with Al, Cu, and Ti but forms a *p*-type Schottky barrier when supported on Ag, Au, Cr, and Pd surfaces; the CIP model is shown in Fig. 9.

Anode material

In a similar vein to metal-ion batteries, by employing DFT calculations, Xiao et al. [35] predicted PG as a promising anode material for lithium and sodium ions batteries. They found that the adsorption of Li/Na ions occurs on the top of sp^2 hybridized C atoms of PG, leading to improved metallic behavior with electronic conductivity and fast charge/discharge rate (Fig. 9). Furthermore, PG has a large metal ion storage potential for Li/Na ions and exhibits a high capacity of (1489 mAh g^{-1}), a low open-circuit voltage (0.55/0.32 V), and a fast ion diffusivity with a diffusion energy barrier of (0.17/0.28 eV) for a single Li/Na ion. All of the findings support the authenticity of the PG sheet as a promising anode material with outstanding performance as compared to other 2D materials [177–179].

Gas sensing

The sensing of toxic gases has recently become a hot topic in environmental science as a way to control emissions and ensure the safety of toxic gas production. The key requirements for sensing materials include the detection power, high sensitivity, selectivity, response time, and surface characteristics. Due to the high surface area, effective carrier mobility, and low electrical noise, 2D materials have a lot of potential for gas sensing applications [180]. It was found that PG is the best option for NO_x (x = 1, 2) molecules with sufficient adsorption power and apparent charge transfer. Furthermore, after NO_2 (NO) adsorption, the current-voltage (IV) curves of PG show a massive reduction of 88% (90%) in the current (Fig. 9) [181]. In addition, DFT-based calculations indicate that H_2O, H_2S, CO, and NH_3 act as electron donors while SO_2 and NO as electron acceptors when adsorbed on PG's surface. PG's superior sensing efficiency is

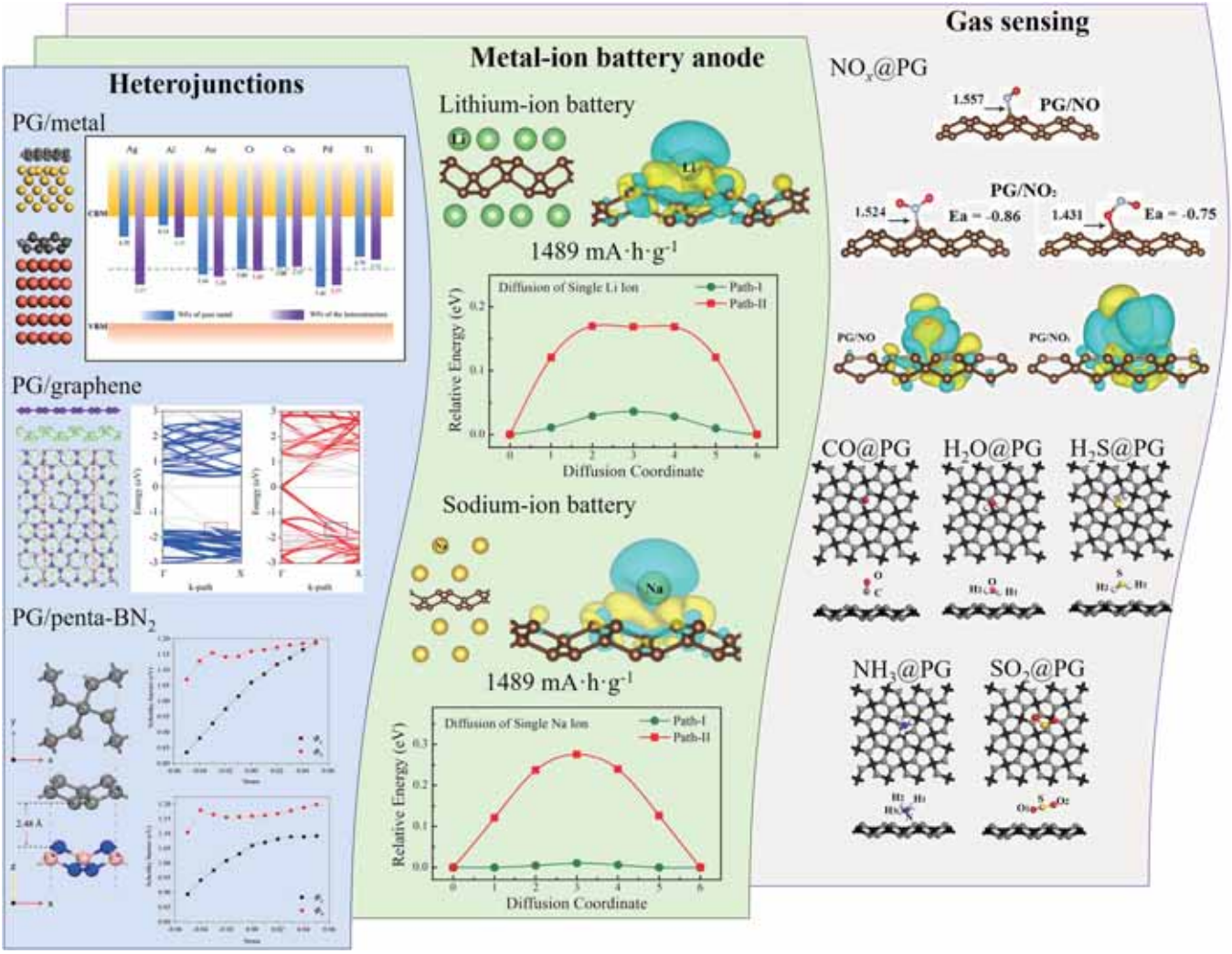

Fig. 9. An overview of theoretically realized potential applications of PG.
Illustrations for "PG/metal" in the "Heterojunctions" panel are adapted with permission from Ref. [176]. Copyright 2019, American Institute of Physics. Illustrations for "PG/graphene" are adapted with permission from Ref. [36]. Copyright 2017, American Institute of Physics. Illustrations for "PG/penta-BN_2" are adapted with permission from Ref. [171]. Copyright 2018, American Institute of Physics. Illustrations in the "Metal-ion battery anode" panel are adapted with permission from Ref. [35]. Copyright 2016, American Chemical Society. Illustrations for "NO_x@PG" in the "Gas sensing" panel are adapted from Ref. [181]. Illustrations for "CO@PG", "H_2O/PG", "H_2S/PG", "NH_3/PG" and "SO_2/PG" are adapted from Ref. [144].

comparable to other 2D materials like graphene and phosphorene [144,182,183].

PG derived structures

Being a rising star of the carbon family, PG not only shows its unique geometry and novel properties but also provides the base for its derived structures, which have also promoted the traditional behavior of its family to design structural analogs in all possible dimensions. As a consequence of such efforts, multiple theoretical reports have shown that the single layer of PG can be tailored to form a variety of pentagonal designs, such as 1D PG nanotubes (PGNTs) by rolling [18], 1D PG nanoribbons (PGNRs) by cutting [6], multilayered 2D structures by stacking [23], functionalized PG by surface modification [24], and diamond-like 3D structures by stacking [18], as shown in Fig. 10. Inspired by these findings, this section reviews the fundamental characteristics of PG-derived structures and their progress in terms of electronic, mechanical, and thermal properties.

Penta-nanotubes

The past decades have witnessed an increasing research enthusiasm for 1D tubular structures due to their fascinating properties and applications in many scientific and technological areas. Practically, this gradual shift from bulk to dimensionally confined 1D systems is mainly driven by the CNTs, which are primarily known for their existence in different chiralities and a wealth of chirality-dependent physical, electrical, and mechanical properties [185–188].

Inspired by the novel performance of CNTs, PG was also expected to have multiple tubular configurations under ambient conditions. From the perspective of morphology, (n, m) PGNTs can be defined as $C_{nm} = na_1 + ma_2$. Here, a_1, a_2 are the lattice vectors, and n, m are the integers to indicate the number of lattice vectors in the five-membered crystal system [18,189,190]. The first study on penta-nanotubes was performed by Zhang et al. in their pioneer work [18]. They found when rolled up, PG can form various fused-pentagon-based nanotubes, named penta-tubes, and the (n, n) PGNTs ($n = 2–8$) are all dynamically and thermally stable and can withstand high temperatures up to 1000 K. More interestingly, they demonstrated that such PGNTs inherit the semiconducting feature of PG, they are all

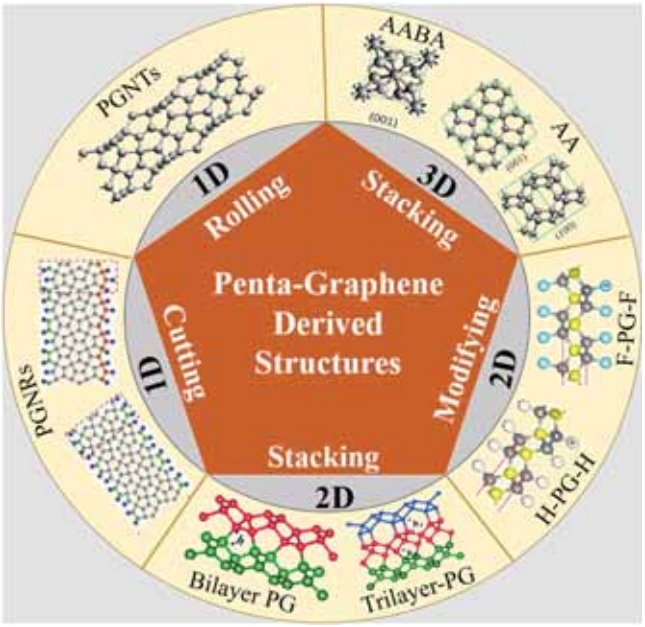

Fig. 10. An atlas of PG-derived structures including PG-nanotubes (PGNTs), PG-nanoribbons (PGNRs), bilayer and trilayer phases of PG, hydrogenated PG (H-PG-H) and fluorinated PG (F-PG-F), and stacked 2D structures by the AA and ABAA stacking. Illustrations for "1D Rolling" and "3D Stacking" are adapted with permission from Ref. [18]. Copyright 2015, National Academy of Science. Illustrations for "2D Modifying" are adapted with permission from Ref. [24]. Copyright 2016, Royal Society of Chemistry. Illustrations for "2D Stacking" are adapted with permission from Ref. [119]. Copyright 2018, Royal Society of Chemistry. Illustrations for "1D Cutting" are adapted with permission from Ref. [184]. Copyright 2018, Elsevier.

semiconducting with medium-size energy band gaps from 1.738 to 2.608 eV, and the band gaps are insensitive to their diameters [18]. This is different from the conventional carbon nanotubes, which have chirality-dependent conductance; namely, they can be metallic or semiconducting depending on their chirality. Notably, this feature could knob barrierless potential of PGNTs in nanoelectronic devices and electrical applications. It is also worthy to note that various direct phase models may also have different stability criteria depending on applied environments. Later on, several follow-up studies suggested that pentagon-based tubular structures can be converged with $n = m$ integers only [18,189] and declared (7,7) format as the most stable configuration among all the explored direct phase models [191,192].

Mechanically, the elastic modulus of PGNTs is reported up to 1000 GPa [192–195], which is quite comparable to typical CNTs [196]. In addition, several other exceptional features such as the auxeticity at ambient conditions, the ultimate tensile stress of 85–110 GPa, and critical strain up to 25% have confirmed the mechanical superiority of PGNTs [188,192] to other conventional CNTs. In contrast to electronic performance, the fracture patterns of PGNTs strongly depend on the chirality of the nanotubes. In this manner, Sousa et al. [194] have shown that the armchair-type PGNTs are suddenly fractured at lower tensile strain values due to differences in bonding alignments as compared to zigzag-type PGNTs. Interestingly, PGNTs can be in direct α-phase and inverted β-phase, corresponding to the inner dimers parallel or perpendicular to the main axis of the tube [197]. It was found that the β-phase is thermodynamically unstable and transforms to a lower energetic γ-phase at higher temperature intervals [197].

Beyond these intrinsic features, several tuning strategies (strain engineering, diameter ranges, etc.) have also been adopted to improve the structural performance of PGNTs and to enhance their electronic and mechanical tunability under applied conditions. Wang et al. [197] combined DFT and MD simulations to explore the strain impacts on the electronic properties of PGNTs, and found that compressive strain decreases the electronic bandgap while tensile strain (under 6% coverage) increases the bandgap of PGNTs. Furthermore, they also determined that compressive strain can drive semiconductors to metal transitions in β-phase (4,4), (5,5), and (6,6) tubes [197]. By combining DFT and reactive MD simulations, Sousa et al. [192] showed that (11,11) β-phase PGNT experiences a structural transition to (11,11) α-phase under tensile stretching at room conditions. Zhao and co-workers [189] revealed that the electronic bandgap of PGNTs is slightly reduced by increasing the diameter of the nanotubes. Beyond the bandgap performance, higher elasticity of PGNTs is observed with a failure strain of > 60% under tensile strain engineering [195]. Beyond this range, these tubes behave plastically due to the irreversible structural transition of carbon rings from pentagons to polygons (trigons, tetragons, hexagons, etc.) [195].

Penta-nanoribbons

Besides the 1D-tubular structures, multiple types of PGNRs, including zigzag (ZZ), armchair (AA), zigzag-armchair (ZA), and sawtooth (SS), have been determined by cutting the single layer of PG along the various crystallographic orientations [20–22]. Among them, sawtooth PGNRs (Fig. 10) have captivated considerable attention due to their exciting structural features and applications. For example, pristine sawtooth PGNRs are found to be more stable semiconductors than the other three phases, which exhibit metallic nature at room conditions [7,198]. Although the intrinsic bandgap of sawtooth PGNRs (~ 0.7–2.6 eV) [7,20,21,198,199] is smaller than monolayer PG due to quantum confinement and edge effects.

Fortunately, the electronic, optical, and transport properties of sawtooth PGNRs can be tuned by chemical doping and edge modifications. The edge modified/terminated sawtooth PGNRs are found with n-type semiconducting nature, promoting very high carrier mobility up to 10^4 cm^2/Vs [184,198]. In this regard, Tien et al. [21] found that the current intensity of sawtooth PGNRs can be increased up to 9 orders of magnitude after the chemical doping of N and P atoms. In another study, they reported that the edge-modifications of sawtooth PGNRs by P or Si combined with H atoms also promote the current magnitude up to 10^9 times due to increased mobile electrons and transport vacancies [22]. Wu et al. [198] found that the Al-based edge modifications convert n-type sawtooth PGNRs semiconductors to p-type and also extend the absorption efficiency of these models from visible to ultraviolet regions. These results suggest broader applications of sawtooth PGNRs in optoelectronics, spin electronics, and solar devices.

Besides the intriguing performance of sawtooth PGNRs, the edge modifications of PGNRs with non-metallic atoms (H, N, P, O, S, F, Si, etc.) can drive the bandgap transitions from semiconductor to metal, semi-metal, or quasi-metals, respectively [22,184]. The increasing bandwidth marginally reduces the bandgap of PGNRs [6], but these models tend to attain the bandgap of PG monolayer at a ribbon width of 8 stripes [200]. Yuan et al. [7] reported that an applied transverse electric field promotes magnetism in PGNRs and transforms magnetic semiconductors to half-metallic wide bandgap materials. Furthermore, DFT simulations have suggested that the electronic bandgap of PGNRs is reduced under applied tensile and bending strain [6,199], and mechanically, these structures can tolerate a tensile loading up to 11.5% [6].

Multilayered PG

In recent years, 2D layered materials have sparked immense interest in fundamental physics and applied sciences due to their enhanced and highly tunable properties [201,202]. Interestingly, these materials can be developed by stacking their monolayers via van der Waals forces and stacking alignments, etc., resulting in

structural reliability for promoting their performance intrinsically or extrinsically under applied conditions. With the development of modern sciences, several stacking strategies, such as direct stacking, stacking misalignment, and stacking fault, have been proposed to design multilayered 2D sheets.

PG can also form layered structures with tunable features, as shown in Fig. 10. It was found that multi-layered PG display dramatically different features from their mother phase, PG. For example, in bilayer (AA and AB) PG models, the AA stacking sequence has mirror-symmetry with respect to the middle plane of the two layers, which is energetically more stable than the AB stacked configuration [136]. And for AB stacking sequence, the upper layer deviates from the mirror image of the bottom layer by around $a/2$. On the other hand, tri-layer (AAA, ABA, AAB) stacked PG models are observed as totally asymmetric and found insensitive to stacking configuration [119].

Based on DFT calculations, Yu et al. [23] predicted the multi-layer and stacked PG models and reported that the bandgap of a few-layer PG is reduced to 2.57 eV from 3.27 eV at the HSE06 level when the number of layers is greater than four, showing a weak dependence on the layer thickness. While for the AA and AB stacking sequence, the bandgap values are 2.8 eV and 1.37 eV, respectively, based on the stacking misalignment rule. Wang et al. [119] investigated the semiconducting characteristics of the bilayer and trilayer PG phases by using DFT simulations and determined the insensitive responses of these phases to the applied stacking sequence. Moreover, they found that external electric field strength can produce the Stark effect in these models and reduce the bandgap.

Along with the novel/tunable electronic properties of PG's multilayer phases, their thermal properties have also drawn significant attention at ambient and artificial conditions. In this regard, Sun et al. [134] have proposed that the thermal conductivity of bilayer PG can be reached to 563 W/mK (at 300 K) by applying DFT-D vdW functionals. Furthermore, they also revealed that the applied strain (beyond 10% coverage) reduces the thermal conductivity of bilayer PG up to 87% as compared to the unstrained format. This reduction is ascribed to enhanced phonon anharmonicity of phonon modes having ultra-low frequency under applied strained environment [134].

Functionalized PG

In PG, the sp^2 hybridized C atoms provide the base for chemical functionalizations, such as hydrogenation, fluorination, and hydro-fluorination. In this light, Li et al. [24] used hydrogen and fluorine atoms (Fig. 10) to reveal the impact of surface functionalizations on the monolayer PG sheet. They predicted that fully hydrogenation/fluorination elongates double bonding lengths from 1.34 Å to 1.55 Å for hydrogenated PG and from 1.34 Å to 1.58 Å for fluorinated PG and accordingly transforms them into single bonding configurations. More interestingly, chemical functionalization also tunes the chemical and physical nature of PG by modifying semiconducting to insulating, negative Poisson's values to positive ones, and reducing Young's modulus values [24]. As a result, the whole symmetry of chemically functionalized PG propounds sp^3 type bondings and tries to release internally stored stress [24,25]. Jia et al. [30] also reported their results in almost similar trends for chemically functionalized hydro-fluorinated PG sheets.

Pentagon-based diamond-like structures

The advent of bilayer and trilayer patterns in PG also encouraged the research enthusiasm for atomically stacked 3D pentagonal structures consisting of sp^2 and sp^3 combinations. Apparently, covalently bonded sp^2 C atoms in PG prevent it from being stacked in the same way. But stacking alterations provide the degree of freedom to rationally design 3D pentagonal structures and to control/modulate the exotic properties of derived structures. Zhang et al. [18] modified the stacking sequence of PG layers, resulting in pentacyclic diamond-like structures of carbon, named AA-T12 and ABAA-T24, as shown in Fig. 10. They predicted the wide-bandgap semiconducting nature of these models with bandgap values of 5.68 eV and 5.33 eV, respectively, for AA-T12 and ABAA-T24 carbon phases. Based on these findings, Zhu and Su [203] extended this library by considering the inter-layer covalent bondings in bilayer PG. They proposed that the interlayer spacing between sp^2-hybridized carbon layers can be reduced by sliding AA to AB stacking configuration along the [100] direction in the XY-plane, which leads to chiral pentagonal diamond-like 3D structures with space groups $P6_122$ and $P6_522$. Similar to AA-T12 and ABAA-T24 phases, these structures are also investigated as wide-bandgap semiconductors with a value of 5.7 eV [203]. In addition, in a recent study, Fujii and his co-workers [204] theoretically explored a covalently bonded 3D cubic pentagonal network of sp^2 and sp^3 C atoms within the space group of Fm3m, named "pentadiamond". Further studies have found that pentadiamond possesses an indirect bandgap of 2.46–2.52 eV (at the GGA levels) [204–207] and 3.31–3.58 eV (at the HSE06 level) [205,206] and a high carrier mobility of 351.72 cm^2/Vs at ambient environments [207], and exhibits some other exciting mechanical and thermal features, including Young's and shear moduli up to 522 GPa and 220 GPa [206,208,209], a tensile strength of 60 GPa [206], temperature-dependent and chemically functionalized fracture properties [210,211], and the low thermal conductivity of 427–490.88 W/mK at room temperature [206,212].

The cousins of PG

Penta-silicene: stability, properties, and applications

As the nearest neighbor of carbon in the periodic table, silicon (Si) has been the first candidate chosen for extending the carbon structures to other elements. A well-known example is the silicene sheet [123,213,214], which is the counterpart of graphene with Dirac cone. Following this logic, it is natural to do such extension from penta-C to penta-Silicene. However, it was found that the pristine penta-Silicene sheet with the atomic configuration of PG is dynamically unstable [215], but surface hydrogenation can stabilize penta-Silicene [24]. The resulting hydrogenated penta-silicene sheet is an indirect band-gap semiconductor material with superior flexibility, which can endure large biaxial and uniaxial strains up to 25% and 31%, respectively [216]. While for 1D nanoribbons, the edge states induce flat bands at the Fermi level, causing a spontaneous spin-polarization in the system. In addition, fluorination, lithiation, and multilayer-stacking can also stabilize the penta-Silicene sheet [216–218]. In this section, we review the progress made experimentally and theoretically penta-Silicene and its applications.

Penta-silicene nanoribbons: experimental synthesis

Inspired by the proposal of PG, Jeroge et al. [46] in 2016 reported the pentagonal nature of a perfectly aligned single and double-strand Si-nanoribbons using the extensive DFT and scanning tunneling microscopy (STM) simulations. 1D penta-Silicene nanoribbons were grown on the missing row reconstructed on Ag (110) surface (Fig. 11a-b). Later on, Geoffroy et al. [47] carried out systematic studies to further validate the pentamer model of silicene grown on the reconstructed surface by combined grazing incidence x-ray diffraction (GIXD), STM, and DFT calculations (Fig. 11c). In 2018, Sheng et al. [219] reported penta-Silicene nanoribbons and magic clusters on Ag (110), which fits perfectly to the pentamer model (Fig. 11d-g) by using non-contact atomic force microscopy (nc-AFM) and tip-enhanced Raman spectroscopy (TERS). All of these studies

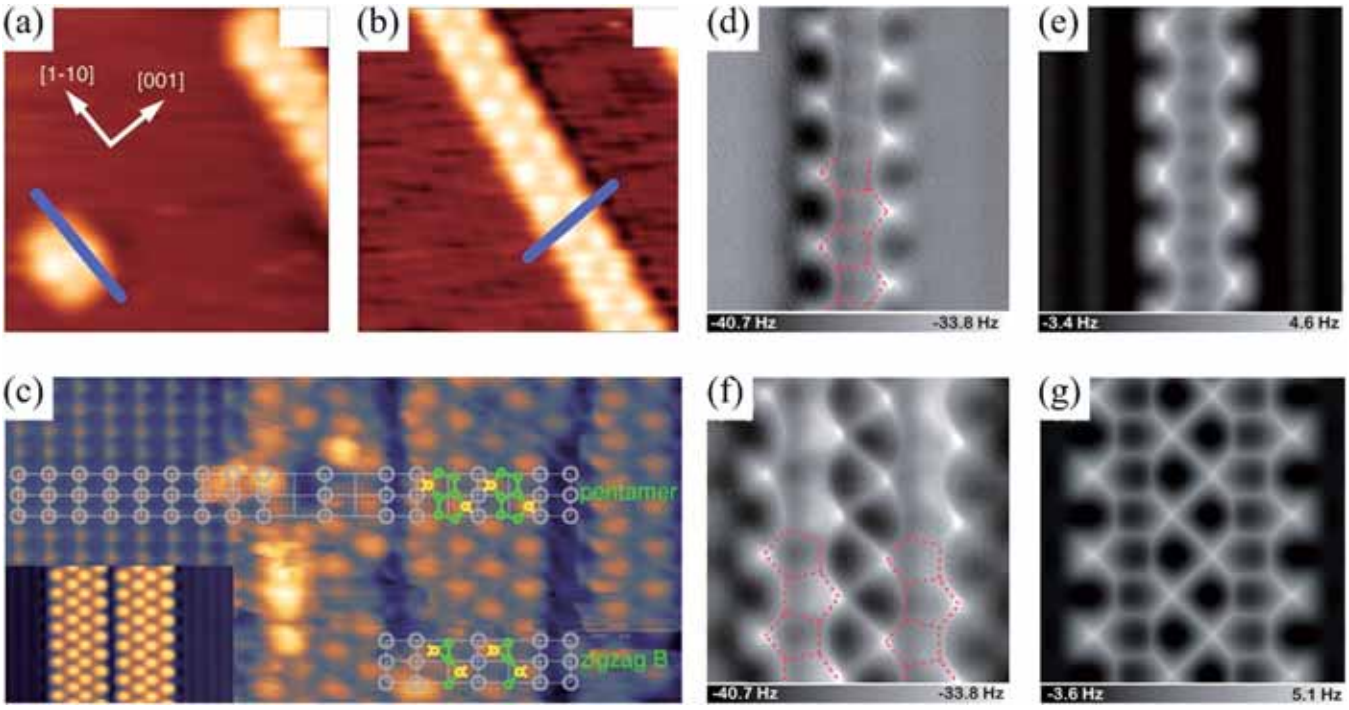

Fig. 11. (a, b) STM images of (5.3×5.3 nm^2) silicene nanodot and a single nanoribbon. (c) STM high-resolution image (4.5×9 nm^2) of penta-silicene embedded on Ag(110) surface. (d, f) Experimental, and (e, g) simulated STM images of penta-silicene single- and double-nanoribbon models.
(a, b) Adapted from Ref. [46]. (c) Adapted with permission from Ref. [47]. Copyright 2016, American Physical Society; (d–g) Adapted with permission from Ref. [219]. Copyright 2018, American Chemical Society.

show the feature of the pentagonal configuration of Si nanoribbon grown on substrates.

Ferroelectricity with high Curie temperature

Previous theoretical studies suggested that the PG-like configuration is not stable for Si, and surface modifications are needed for the stabilization [218]. In contrast, the successful synthesis of penta-Silicene nanoribbons suggested the possibility of finding a stable configuration of the penta-Silicene sheet. By employing DFT simulations, Guo et al. [220] demonstrated that tilting Si_3-dimers within the confined lattice could stabilize penta-Silicene, and this helps in the reduction of Coulomb repulsion within the charged Si atoms (Fig. 12a-b). They have named this stable configuration as *T* penta-silicene. The electronic properties show that *T* penta-silicene is a quasi-direct bandgap semiconductor with a bandgap value of 0.65 eV (Fig. 12c), different from the zero bandgap feature of silicene [213] that restricts its application in electronic devices such as information storage devices. Moreover, by applying Berry phase theory, they further showed that the tilting of Si_3-dimers leads to rigorous electric polarization between two nonequivalent Si_3 atoms with an in-plane polarization value of 18.7 pC/m in the *x*-direction, while zero in the *z*-direction, as shown in Fig. 12d. Thus, *T* penta-silicene exhibits in-plane ferroelectricity. Based on Landau-Ginzburg's theory, the Curie temperature was found to be as high as 1190 K, as shown in Fig. 12e. This study has further extended to other penta-structures like penta-BCN and penta-CNP [44,45].

Low lattice thermal conductivity and high figure of merit

In a recent study, Gao et al. [221] reported an ultra-low lattice thermal conductivity (1.29 W/mK) of monolayer penta-Silicene at room temperature because of the strong anharmonic scattering (Fig. 13a-b). Furthermore, the conversion efficiency improves as the temperature rises. *T* penta-silicene shows remarkable room-temperature *ZT* of 3.4 and 3.0 at the reachable hole and electron concentrations attributed to its ultra-low thermal conductivity 1.66 and 1.29 W/ mK along the *x*- and *y*-axis. The negative poison ratio of *T* penta-silicene is −0.55, which is 5 times larger than that of PG (−0.09). At the carrier concentration of 10^{12} cm^{-2}, the Seebeck coefficient of penta-Silicene is calculated to be 400 μV/K for both *p*- and *n*-type carriers, as shown in Fig. 13c-d. The electronic thermal conductivity has a value of 0.2 W/mK at a concentration lower than 10^{12} cm^{-2}. Interestingly, due to the high-power factor of 156.40 and 40.23 mW/K^2 and low thermal conductivity, *T* penta-silicene shows a large *ZT* (> 2) at room temperature for both *x*- and *y*-axis. Specifically, maximum *ZT* for holes has values of 3.43 and 2.24 at 3.42×10^{12} and 4.60×10^{12} cm^{-2} concentrations along the *x*- and *y*-axis at room temperature, respectively. Similarly, maximum *ZT* for the electrons has values of 2.18 and 3.04 at 2.51×10^{12} and 1.85×10^{12} cm^{-2} along the *x*-and *y*-axis at 300 K, as shown in Fig. 13e-f [222]. The pure-Si sheet exhibits advantages over the traditional thermoelectric materials, such as Bi_2Te_3 or PbTe, which are hazardous to the environment and contain rare elements [222,223] with limited high-temperature stability.

Penta-germanene

After the successful synthesis of silicene in 2012, Dávila et al. [224] synthesized an atom-thin, ordered germanene in situ through germanium molecular beam epitaxy using a gold (111) surface as a substrate similar to the growth of silicene on Ag (111) substrate. Following the idea of penta-Silicene, Jun and Zeng [225] studied the structural stability and electronic properties of penta-germanene (penta-Ge) modulated by chemical functionalization and tensile strain. The geometry of the studied structures is shown in Fig. 14a. The authors proposed that a 2D pentagonal nanosheet of penta-Ge can be stabilized by both hydrogenation and fluorination. Phonon dispersion spectrum and ab initio molecular dynamics simulations demonstrated that the dynamic and thermal stabilities of the two functionalized penta-Ge nanostructures could be maintained even under a high temperature of 500 K. Their calculations revealed that

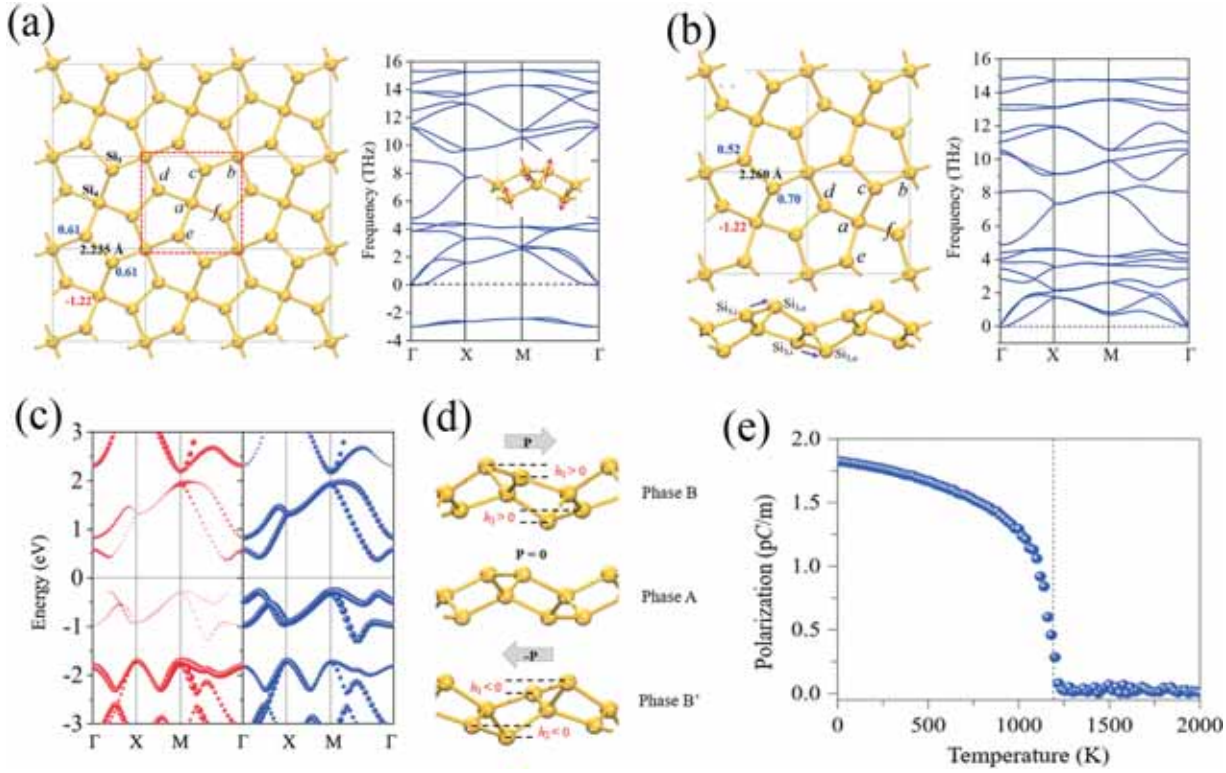

Fig. 12. (a, b) Top and side views and phonon spectra of penta-silicene and *T* penta-silicene, (c) Band structure diagram of *T* penta-silicene, (d) Schematic side views of the two degenerate ferroelectric phases (B and B′) and the nonpolar phase (A).
Adapted with permission from Ref. [220]. Copyright 2019, American Physical Society.

both hydrogenated and fluorinated penta-Ge sheets are semiconductors with indirect band gaps of 1.92 and 1.39 eV (2.60 and 2.09 eV by the hybrid functional), respectively (Fig. 14b). The electronic structures of the functionalized penta-Ge can be effectively modulated by biaxial tensile strain, and an indirect to direct gap transition can be achieved for the hydrogenated penta-Ge sheet by 6% biaxial strain, as shown in Fig. 14c. Moreover, the author explains that the bandgap of the hydrogenated penta-Ge can be modulated from 0.71 to 3.46 eV (1.16–4.35 eV using the HSE06 functional with heteroatom doping of C, Si, Sn, and Pb atoms, suggesting the semiconductor–insulator transition for differently doped nanostructures (Fig. 14d). As a result, the functionalized penta-Ge are expected to have promising applications in nanoelectronics and nanomechanics.

Furthermore, Gao et al. [221] also studied the thermal conductivity and thermal transport properties of monolayer penta-Ge. The geometry of penta-Ge is shown in Fig. 15a. Penta-Ge has a dynamically stable configuration, as shown in Fig. 15b, with a frequency of 250.7 cm^{-1} and a zero gap between acoustic and optical phonons, hence ideal for an ultra-low thermo-conductivity material. According to their study, penta-Ge has the lowest lattice thermal conductivity of (0.30 W/mK) among the 2D crystals at room temperature because of the weak phonon harmonic interaction and strong anharmonic scattering. Fig. 15c shows the calculated thermal conductivity along the *x*-axis and *y*-axis. The recorded value of thermal conductivity is reduced for penta-Ge (0.38 W/mK) along the *x*-axis and (0.30 W/mK) along the *y*-axis; it is different from that of PG, which has an isotropic thermal conductivity of 645 W/mK at 300 K [221]. The study further elaborates that the anharmonic phonon scattering has a large effect on the thermal conductivity and thermal transport properties of a material. The anharmonic phonon scattering can be obtained by Grüneisen parameter γ defined as:

$$\gamma = \frac{d\mathrm{In}\omega}{d\mathrm{In}V} \tag{2}$$

Here ω is the function of band indices and wave vector. Higher the value of γ, higher will be the anharmonicity. The calculated values for anharmonic phonon scattering of penta-Ge show different behavior than PG and have higher values as compared with penta-Silicene (Fig. 15d). penta-Ge shows the highest anharmonicity compared to PG and penta-Silicene.

Conclusions and outlook

Pentagons were considered as topological defects in materials for decades, but are well-known for the mathematical proposition proposed by Karl Reinhardt in 1918, namely, how to cover the Euclidean plane using only identical copies of the same shape pentagons, leaving no gaps and with no overlaps. Fifteen types of irregular pentagons that can tile the Euclidean plane have been proposed during the past more than 100 years. However, the most intriguing question is how to realize these mathematical models in materials. PG provides the answer and stands for a paradigm shift in materials design and synthesis, which motivates many follow-up studies in this field.

In this work, we reviewed the theoretical and experimental progress made in designing and synthesizing 2D pentacyclic materials by focusing on PG and its derivatives, including penta-nanoribbons, penta-nanotubes, multilayered and functionalized PG, for their geometrical configurations, stability, and emerging properties. Discussions are also extended to penta-silicene and penta-germanene, which are considered as the cousins of PG. From C to Si and Ge, their pentagonal sheets are all semiconductors instead of semimetals, while Dirac cones with zero bandgaps are found in their hexagonal counterparts, namely, graphene, silicene, and germanene, and they all have strong anharmonic phonon scattering that leads to low lattice thermal conductivities decreasing in the order of PG > penta-silicene > penta-Ge. These results clearly show the

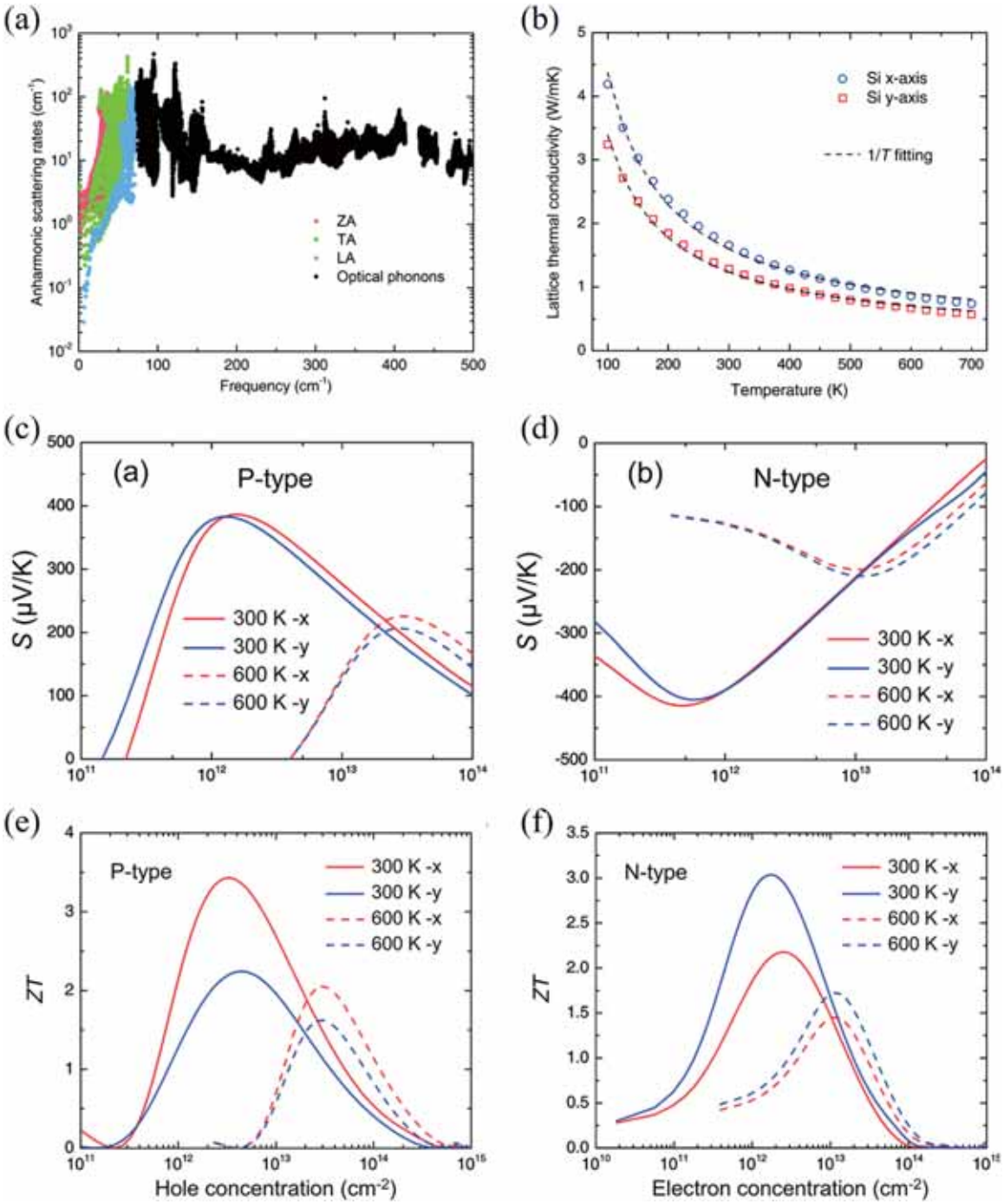

Fig. 13. (a) Calculated an-harmonic scattering rate of penta-Silicene, (b) lattice thermal conductivity of penta-Silicene calculated by using BTE as a function of temperature along *x*- and *y*-axis. (c, d) Temperature-dependent Seebeck coefficient, and (e, f) Figure of merit *ZT*.
(a, b) Adapted with permission from Ref. [221]. Copyright 2019, Royal Society of Chemistry. (c–f) Adapted with permission from Ref. [222]. Copyright 2020, American Chemical Society.

significance of structural units in determining the geometric configuration and physical properties. Therefore, changing the structural building units is the most direct and efficient strategy in the design and synthesis of new materials. The following aspects are worthy of attention for future studies:

(1) Using pentagonal molecules as the precursors to synthesize PG sheet by following the bottom-up route. So far, several such molecules, including cyclopentane, furan, pyrrole, thiophene, terthienyl, and tetrathiafulvalene have been discovered. It is highly desirable to develop technology for assembling these units into PG sheet or designing new precursors for more feasible synthesis. When obeying the top-down route, T12 carbon needs to be synthesized first, then PG sheet can be obtained by chemically exfoliating T12-carbon. It is encouraging to note that T-carbon was theoretically predicted in 2011 and experimentally synthesized in 2017.
(2) Developing advanced strategies for fabricating 2D penta-silicene sheet instead of penta-silicene nanoribbons. It is a well-developed technology to synthesize silicene on different substrates, which shows the hope of synthesizing the penta-analog.

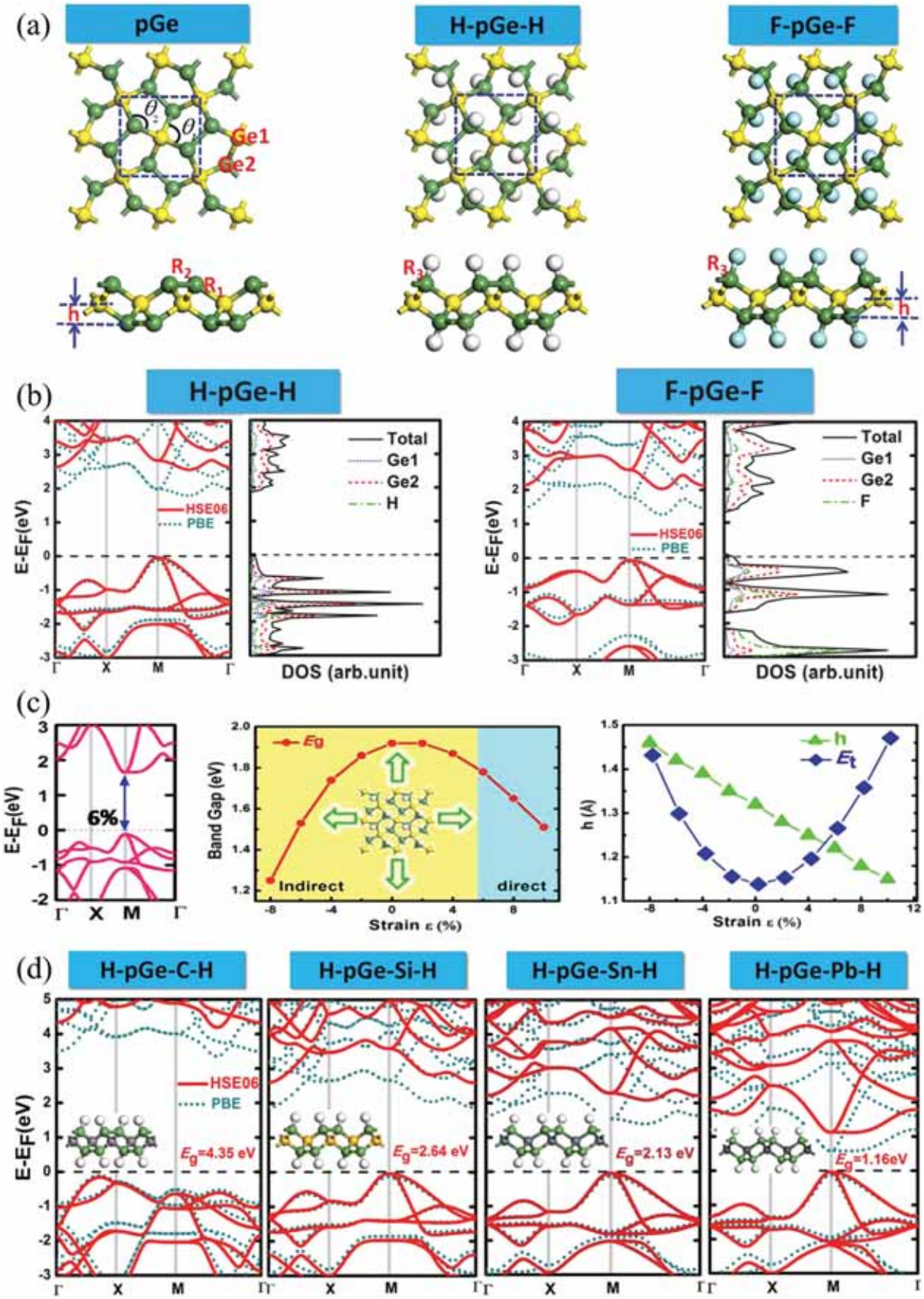

Fig. 14. (a) Top and side views of penta-Ge, hydrogenated penta-Ge (H-pGe-H), and fluorinated penta-Ge (F-pGe-F). (b) Band structures of H-pGe-H and F-pGe-F. (c) Strain modulated band structure of H-pGe-H under 6% strain, and effect of biaxial strain on the bandgap and the buckling distance, respectively. (d) Calculated band structures of the doped H-pGe-H sheets with C, Si, Sn, and Pb, respectively.
Adapted from Ref. [225].

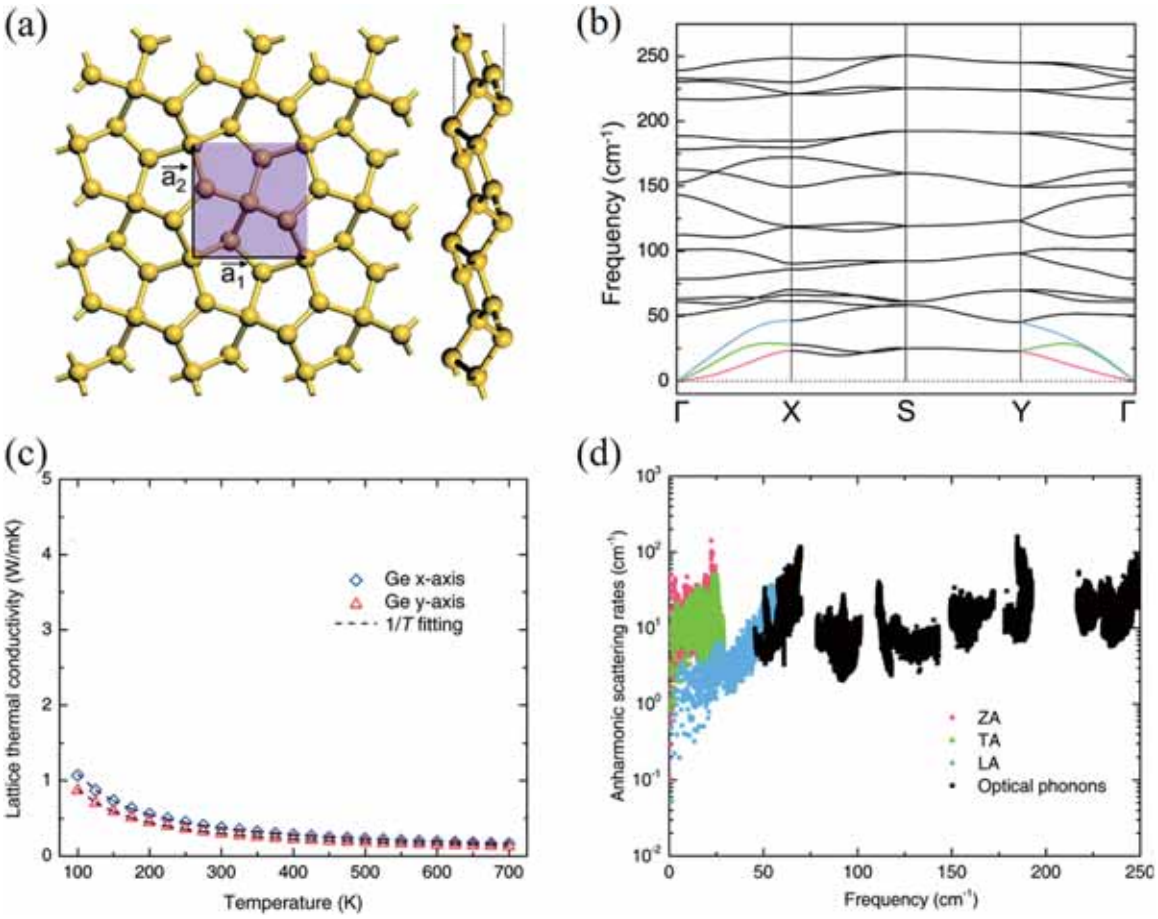

Fig. 15. (a, b) Top and side views of the geometry and phonon spectrum of penta-Ge. (c) Lattice thermal conductivity of penta-Ge calculated using BTE as a function of temperature along the *x*- and *y*-axis. (d) Calculated an-harmonic scattering rate of penta-Ge.
Adapted with permission from Ref. [221]. Copyright 2019, Royal Society of Chemistry.

(3) Using penta-sheets as the building units to assemble layered and non-layered 3D materials with desired properties. Parallel to the expansion from 2D graphene to 3D graphene monoliths, pentagonal sheets can also be used to design and synthesize 3D materials with additional features.
(4) Although C, Si, and Ge are in the same group in the periodic table of elements, they are different in atomic size and in the flexibility of orbital hybridization, which results in different geometrical configurations and properties. For example, C can form a stable fullerene cage and flat graphene sheet, while Si and Ge can't. Penta-silicene sheet and penta-Ge are unstable in PG configuration, while they become stable in a tilting configuration due to the reduced Coulomb interactions due to their different bonding features. It would be interesting to study if penta-Pb is stable in the tilted penta-Silicene geometry.
(5) Developing algorithms to effectively search for the combinations of the elements that can form a stable multi-element-based penta-sheet. Among the currently reported penta-sheets, the number of elements is less than four. More candidates can be expected with more chemical species in different configurations, based on which, more 3D penta-materials can be further designed going beyond the existing ones. By following the strategy of atomic transmutation, namely, substituting certain types of elements with their neighboring elements in the periodic table for enhanced or newly induced properties, more pentagon-based materials consisting of multiple elements can be obtained.

In conclusion, PG provides a new structural model for 2D materials, while pentagon-based materials represent a new paradigm shift in materials design and synthesis, and have significantly expanded the 2D materials family with exotic features and great potential for device applications. The in-depth study of pentagon-based materials would richen the structure-property relationship, and shed lights on developing functional materials.

Declaration of Competing Interest

The authors declare that they have no known competing financial interests or personal relationships that could have appeared to influence the work reported in this paper.

Acknowledgments

This work is partially supported by grants from the National Natural Science Foundation of China (Grant No. NSFC-11974028), the National Key Research and Development Program of the Ministry of Science and Technology of the People's Republic of China (2017YFA0205003). It is also supported by the high-performance computing platform of Peking University, China.

References

[1] A. Page, F. Ding, S. Irle, K. Morokuma, Insights into carbon nanotube and graphene formation mechanisms from molecular simulations: a review, Rep. Prog. Phys. 78 (2015) 036501.

[2] A. Armano, S. Agnello, Two-dimensional carbon: a review of synthesis methods, and electronic, optical, and vibrational properties of single-layer graphene, Chin. J. Carbon Res. 5 (2019) 67.
[3] K.S. Novoselov, A.K. Geim, S.V. Morozov, D. Jiang, Y. Zhang, S.V. Dubonos, I.V. Grigorieva, A.A. Firsov, Electric field effect in atomically thin carbon films, Science 306 (2004) 666–669.
[4] S. Iijima, Helical microtubules of graphitic carbon, Nature 354 (1991) 56–58.
[5] H.W. Kroto, J.R. Heath, S.C. O'Brien, R.F. Curl, R.E. Smalley, C_{60}: buckminsterfullerene, Nature 318 (1985) 162–163.
[6] B. Rajbanshi, S. Sarkar, B. Mandal, P. Sarkar, Energetic and electronic structure of penta-graphene nanoribbons, Carbon 100 (2016) 118–125.
[7] P. Yuan, Z. Zhang, Z. Fan, M. Qiu, Electronic structure and magnetic properties of penta-graphene nanoribbons, Phys. Chem. Chem. Phys. 19 (2017) 9528–9536.
[8] J. De Sousa, A. Aguiar, E. Girão, A.F. Fonseca, A. Souza Filho, D. Galvão, Computational study of elastic, structural stability and dynamics properties of penta-graphene membrane, Chem. Phys. 542 (2021) 111052.
[9] S. Sahu, G. Rout, Band gap opening in graphene: a short theoretical study, Int. Nano Lett. 7 (2017) 81–89.
[10] P. Silvestrelli, A. Ambrosetti, Bandgap opening in graphene using alkali ions by first principles, Appl. Phys. Lett. 113 (2018) 211603.
[11] J.-S. Park, H.J. Choi, Band-gap opening in graphene: a reverse-engineering approach, Phys. Rev. B 92 (2015) 045402.
[12] D.Q. Khoa, C.V. Nguyen, L.M. Bui, H.V. Phuc, B.D. Hoi, N.V. Hieu, V.Q. Nha, N. Huynh, L.C. Nhan, N.N. Hieu, Opening a band gap in graphene by C–C bond alternation: a tight binding approach, Mater. Res. Express 6 (2019) 045605.
[13] F. Ke, Y. Chen, K. Yin, J. Yan, H. Zhang, Z. Liu, S.T. John, J. Wu, H.-k. Mao, B. Chen, Large bandgap of pressurized trilayer graphene, Proc. Natl. Acad. Sci. USA 116 (2019) 9186–9190.
[14] K. Reinhardt, About the Division of the Plane Into Polygons, Frankfurt, Germany, 1918.
[15] L. Liu, I. Kankam, H.L. Zhuang, Ab initio playing of pentagonal puzzles, Electron. Struct. 1 (2018) 015004.
[16] H.L. Zhuang, From pentagonal geometries to two-dimensional materials, Comput. Mater. Sci. 159 (2019) 448–453.
[17] R.B. Kershner, On paving the plane, Am. Math. Mon. 75 (1968) 839–844.
[18] S. Zhang, J. Zhou, Q. Wang, X. Chen, Y. Kawazoe, P. Jena, Penta-graphene: a new carbon allotrope, Proc. Natl. Acad. Sci. USA 112 (2015) 2372–2377.
[19] H. Prinzbach, A. Weiler, P. Landenberger, F. Wahl, J. Wörth, L.T. Scott, M. Gelmont, D. Olevano, Bv Issendorff, Gas-phase production and photoelectron spectroscopy of the smallest fullerene, C_{20}, Nature 407 (2000) 60–63.
[20] V. Van, On, L.N. Thanh, N.T. Tien, The electronic properties and electron transport of sawtooth penta-graphene nanoribbon under uniaxial strain: ab-initio study, Philos. Mag. 100 (2020) 1834–1848.
[21] N.T. Tien, P.T.B. Thao, V.T. Phuc, R. Ahuja, Electronic and transport features of sawtooth penta-graphene nanoribbons via substitutional doping, Phys. E Low-Dimens. Syst. Nanostruct. 114 (2019) 113572.
[22] N.T. Tien, P.T.B. Thao, V.T. Phuc, R. Ahuja, Influence of edge termination on the electronic and transport properties of sawtooth penta-graphene nanoribbons, J. Phys. Chem. Solids 146 (2020) 109528.
[23] Z.G. Yu, Y.-W. Zhang, A comparative density functional study on electrical properties of layered penta-graphene, J. Appl. Phys. 118 (2015) 165706.
[24] X. Li, S. Zhang, F.Q. Wang, Y. Guo, J. Liu, Q. Wang, Tuning the electronic and mechanical properties of penta-graphene via hydrogenation and fluorination, Phys. Chem. Chem. Phys. 18 (2016) 14191–14197.
[25] Y. Zhang, Q. Pei, Z. Sha, Y. Zhang, H. Gao, Remarkable enhancement in failure stress and strain of penta-graphene via chemical functionalization, Nano Res. 10 (2017) 3865–3874.
[26] H. Einollahzadeh, R. Dariani, S. Fazeli, Computing the band structure and energy gap of penta-graphene by using DFT and G_0W_0 approximations, Solid State Commun. 229 (2016) 1–4.
[27] T. Stauber, J.I. Beltrán, J. Schliemann, Tight-binding approach to penta-graphene, Sci. Rep. 6 (2016) 1–8.
[28] H. Sun, S. Mukherjee, C.V. Singh, Mechanical properties of monolayer penta-graphene and phagraphene: a first-principles study, Phys. Chem. Chem. Phys. 18 (2016) 26736–26742.
[29] Z. Wang, F. Dong, B. Shen, R. Zhang, Y. Zheng, L. Chen, S. Wang, C. Wang, K. Ho, Y.-J. Fan, Electronic and optical properties of novel carbon allotropes, Carbon 101 (2016) 77–85.
[30] H.-J. Jia, H.-M. Mu, J.-P. Li, Y.-Z. Zhao, Y.-X. Wu, X.-C. Wang, Piezoelectric and polarized enhancement by hydrofluorination of penta-graphene, Phys. Chem. Chem. Phys. 20 (2018) 26288–26296.
[31] W. Xu, G. Zhang, B. Li, Thermal conductivity of penta-graphene from molecular dynamics study, J. Chem. Phys. 143 (2015) 154703.
[32] F.Q. Wang, J. Yu, Q. Wang, Y. Kawazoe, P. Jena, Lattice thermal conductivity of penta-graphene, Carbon 105 (2016) 424–429.
[33] R. Krishnan, W.-S. Su, H.-T. Chen, A new carbon allotrope: penta-graphene as a metal-free catalyst for CO oxidation, Carbon 114 (2017) 465–472.
[34] J.I.G. Enriquez, C.V. Al Rey, Hydrogen adsorption on pristine, defected, and 3d-block transition metal-doped penta-graphene, Int. J. Hydrog. Energy 41 (2016) 12157–12166.
[35] B. Xiao, Y.-c. Li, X.-f. Yu, J.-b. Cheng, Penta-graphene: a promising anode material as the Li/Na-ion battery with both extremely high theoretical capacity and fast charge/discharge rate, ACS Appl. Mater. Interfaces 8 (2016) 35342–35352.
[36] Y. Guo, F.Q. Wang, Q. Wang, An all-carbon vdW heterojunction composed of penta-graphene and graphene: tuning the Schottky barrier by electrostatic gating or nitrogen doping, Appl. Phys. Lett. 111 (2017) 073503.
[37] F. Li, K. Tu, H. Zhang, Z. Chen, Flexible structural and electronic properties of a pentagonal B_2C monolayer via external strain: a computational investigation, Phys. Chem. Chem. Phys. 17 (2015) 24151–24156.
[38] A. Lopez-Bezanilla, P.B. Littlewood, Σ–π-band inversion in a novel two-dimensional material, J. Phys. Chem. C 119 (2015) 19469–19474.
[39] S. Zhang, J. Zhou, Q. Wang, P. Jena, Beyond graphitic carbon nitride: nitrogen-rich penta-CN_2 sheet, J. Phys. Chem. C 120 (2016) 3993–3998.
[40] M. Naseri, Arsenic carbide monolayer: first principles prediction, Appl. Surf. Sci. 423 (2017) 566–570.
[41] M. Abutalib, A new antimony carbide monolayer: an indirect semiconductor with a tunable band gap, Chem. Phys. Lett. 708 (2018) 188–193.
[42] M. Naseri, S. Lin, J. Jalilian, J. Gu, Z. Chen, Penta-P_2X (X= C, Si) monolayers as wide-bandgap semiconductors: a first principles prediction, Front. Phys. 13 (2018) 138102.
[43] M. Naseri, Penta-SiC_5 monolayer: a novel quasi-planar indirect semiconductor with a tunable wide band gap, Phys. Lett. A 382 (2018) 710–715.
[44] K. Zhao, Y. Guo, Y. Shen, Q. Wang, Y. Kawazoe, P. Jena, Penta-BCN: a new ternary pentagonal monolayer with intrinsic piezoelectricity, J. Phys. Chem. Lett. 11 (2020) 3501–3506.
[45] W. Sun, Y. Shen, Y. Guo, Y. Chen, Q. Wang, 1, 2, 4-Azadiphosphole-based piezoelectric penta-CNP sheet with high spontaneous polarization, Appl. Surf. Sci. 554 (2021) 149499.
[46] J.I. Cerdá, J. Sławińska, G. Le Lay, A.C. Marele, J.M. Gómez-Rodríguez, M.E. Dávila, Unveiling the pentagonal nature of perfectly aligned single-and double-strand Si nano-ribbons on Ag (110), Nat. Commun. 7 (2016) 1–7.
[47] G. Prévot, C. Hogan, T. Leoni, R. Bernard, E. Moyen, L. Masson, Si nanoribbons on Ag (110) studied by grazing-incidence x-ray diffraction, scanning tunneling microscopy, and density-functional theory: evidence of a pentamer chain structure, Phys. Rev. Lett. 117 (2016) 276102.
[48] Y.P. Shen, Q. Wang, Database for Pentagon-Based Sheets. ⟨http://www.pubsd.com/⟩.
[49] A.D. Oyedele, S. Yang, L. Liang, A.A. Puretzky, K. Wang, J. Zhang, P. Yu, P.R. Pudasaini, A.W. Ghosh, Z. Liu, $PdSe_2$: pentagonal two-dimensional layers with high air stability for electronics, J. Am. Chem. Soc. 139 (2017) 14090–14097.
[50] M. Bykov, E. Bykova, A.V. Ponomareva, F. Tasnadi, S. Chariton, V.B. Prakapenka, K. Glazyrin, J.S. Smith, M.F. Mahmood, I.A. Abrikosov, Realization of an ideal cairo tessellation in nickel diazenide NiN_2: high-pressure route to pentagonal 2D materials, ACS Nano 15 (2021) 13539–13546.
[51] R. Moffett, Cyclopentadiene and 3-chlorocyclopentene-cyclopentene, 3-chloro, Org. Synth. 32 (1952) 41–44.
[52] T. Bally, S. Chai, M. Neuenschwander, Z. Zhu, Pentalene: formation, electronic, and vibrational structure, J. Am. Chem. Soc. 119 (1997) 1869–1875.
[53] A. Meijere, P. Schreiner, The radical anion of acepentalene, Chem. Commun. (1999) 2189–2190.
[54] J. Lahiri, Y. Lin, P. Bozkurt, I.I. Oleynik, M. Batzill, An extended defect in graphene as a metallic wire, Nat. Nanotechnol. 5 (2010) 326–329.
[55] G.R. Berdiyorov, M.E.-A. Madjet, First-principles study of electronic transport and optical properties of penta-graphene, penta-SiC_2 and penta-CN_2, RSC Adv. 6 (2016) 50867–50873.
[56] S. Bravo, J. Correa, L. Chico, M. Pacheco, Symmetry-protected metallic and topological phases in penta-materials, Sci. Rep. 9 (2019) 1–14.
[57] C.-P. Chen, C. Liu, L.-L. Liu, L.-S. Zhao, X.-C. Wang, Enhanced thermoelectric properties of penta-graphene by strain effects process, Mater. Res. Express 4 (2017) 105031.
[58] J. Chen, H. Cui, P. Wang, Y. Zheng, D. Wang, H. Chen, H. Yuan, Band gap and magnetic engineering of penta-graphene via adsorption of small transition clusters, Phys. Chem. Chem. Phys. 22 (2020) 26155–26166.
[59] S. Bravo, J. Correa, L. Chico, M. Pacheco, Tight-binding model for opto-electronic properties of penta-graphene nanostructures, Sci. Rep. 8 (2018) 1–10.
[60] S. Winczewski, M.Y. Shaheen, J. Rybicki, Interatomic potential suitable for the modeling of penta-graphene: molecular statics/molecular dynamics studies, Carbon 126 (2018) 165–175.
[61] W. Tu, K. Wang, L. Qin, Z. Sun, J. Chen, Intrinsic mechanical properties and fracture mechanism of monolayer penta-graphene investigated by nanoindentation: a molecular dynamics study, Comput. Mater. Sci. 169 (2019) 109145.
[62] S. Winczewski, J. Rybicki, Anisotropic mechanical behavior and auxeticity of penta-graphene: molecular statics/molecular dynamics studies, Carbon 146 (2019) 572–587.
[63] W. Zhang, C. Chai, Q. Fan, Y. Song, Y. Yang, Two-dimensional carbon allotropes with tunable direct band gaps and high carrier mobility, Appl. Surf. Sci. 537 (2021) 147885.
[64] O. Rahaman, B. Mortazavi, A. Dianat, G. Cuniberti, T. Rabczuk, Metamorphosis in carbon network: from penta-graphene to biphenylene under uniaxial tension, FlatChem 1 (2017) 65–73.
[65] J. Zhang, R. Wang, X. Zhu, A. Pan, C. Han, X. Li, D. Zhao, C. Ma, W. Wang, H. Su, Pseudo-topotactic conversion of carbon nanotubes to T-carbon nanowires under picosecond laser irradiation in methanol, Nat. Commun. 8 (2017) 1–7.
[66] H. Prinzbach, A. Weiler, P. Landenberger, F. Wahl, J. Wörth, L.T. Scott, M. Gelmont, D. Olevano, Gas-phase production and photoelectron spectroscopy of the smallest fullerene, C_{20}, Nature 407 (2000) 60–63.

[67] K. Kaiser, L.M. Scriven, F. Schulz, P. Gawel, L. Gross, H.L. Anderson, An sp-hybridized molecular carbon allotrope, cyclo[18] carbon, Science 365 (2019) 1299–1301.
[68] M.-Q. Le, Mechanical properties of penta-graphene, hydrogenated penta-graphene, and penta-CN_2 sheets, Comput. Mater. Sci. 136 (2017) 181–190.
[69] C. Zhang, Y. Cao, X. Dai, X.-Y. Ding, L. Chen, B.-S. Li, D.-Q. Wang, Ab-initio study of the electronic and magnetic properties of boron-and nitrogen-doped penta-graphene, Nanomaterials 10 (2020) 816.
[70] B. Li, Z.-G. Shao, Adsorption of DNA/RNA nucleobases and base pairs on penta-graphene from first principles, Appl. Surf. Sci. 512 (2020) 145635.
[71] V. Van Thanh, N.T. Hung, Charge-induced electromechanical actuation of two-dimensional hexagonal and pentagonal materials, Phys. Chem. Chem. Phys. 21 (2019) 22377–22384.
[72] M. Yagmurcukardes, H. Sahin, J. Kang, E. Torun, F. Peeters, R. Senger, Pentagonal monolayer crystals of carbon, boron nitride, and silver azide, J. Appl. Phys. 118 (2015) 104303.
[73] T. Han, S. Cao, X. Wang, Z. Xue, X. Zhang, Mechanical behaviours of penta-graphene and effects of hydrogenation, Mater. Res. Express 6 (2019) 085612.
[74] S.W. Cranford, When is 6 less than 5? Penta-to hexa-graphene transition, Carbon 96 (2016) 421–428.
[75] C. Lee, X. Wei, J.W. Kysar, J. Hone, Measurement of the elastic properties and intrinsic strength of monolayer graphene, Science 321 (2008) 385–388.
[76] M.E. Kilic, K.-R. Lee, Penta carbides: two-dimensional group-IV semiconductors containing C2 dimers for nanoelectronics and photocatalytic water splitting, Phys. Rev. Mater. 5 (2021) 065404.
[77] C.P. Ewels, X. Rocquefelte, H.W. Kroto, M.J. Rayson, P.R. Briddon, M.I. Heggie, Predicting experimentally stable allotropes: Instability of penta-graphene, Proc. Natl. Acad. Sci. USA 112 (2015) 15609–15612.
[78] Y. Zhang, Q. Pei, C. Wang, Mechanical properties of graphynes under tension: a molecular dynamics study, Appl. Phys. Lett. 101 (2012) 081909.
[79] O. Leenaerts, H. Peelaers, A. Hernández-Nieves, B. Partoens, F. Peeters, First-principles investigation of graphene fluoride and graphane, Phys. Rev. B 82 (2010) 195436.
[80] S.-D. Guo, S.-Q. Wang, Tuning pure out-of-plane piezoelectric effect of penta-graphene: a first-principle study, J. Phys. Chem. Solids 140 (2020) 109375.
[81] H.S. Park, S.Y. Kim, A perspective on auxetic nanomaterials, Nano Converg. 4 (2017) 1–4.
[82] K.E. Evans, Auxetic polymers: a new range of materials, Endeavour 15 (1991) 170–174.
[83] J.-W. Jiang, H.S. Park, Negative poisson's ratio in single-layer black phosphorus, Nat. Commun. 5 (2014) 1–7.
[84] W. Zhang, C. Chai, Q. Fan, Y. Song, Y. Yang, A novel two-dimensional sp-sp^2-sp^3 hybridized carbon nanostructure with a negative in-plane Poisson ratio and high electron mobility, Comput. Mater. Sci. 185 (2020) 109904.
[85] S. Winczewski, J. Rybicki, Negative Poisson's ratio from pentagons: a new auxetic structure combining three different auxetic mechanisms, Comput. Mater. Sci. 201 (2022) 110914.
[86] T. Han, X. Wang, X. Zhang, F. Scarpa, C. Tang, Mechanics of penta-graphene with vacancy defects under large amplitude tensile and shear loading, Nanotechnology 32 (2021) 275706.
[87] Q. Wei, Y. Yang, A. Gavrilov, X. Peng, A new 2D auxetic CN_2 nanostructure with high energy density and mechanical strength, Phys. Chem. Chem. Phys. 23 (2021) 4353–4364.
[88] Q. Pei, Y. Zhang, V. Shenoy, A molecular dynamics study of the mechanical properties of hydrogen functionalized graphene, Carbon 48 (2010) 898–904.
[89] Y. Zhang, W. Jie, P. Chen, W. Liu, J. Hao, Ferroelectric and piezoelectric effects on the optical process in advanced materials and devices, Adv. Mater. 30 (2018) 1707007.
[90] L. Dong, J. Lou, V.B. Shenoy, Large in-plane and vertical piezoelectricity in Janus transition metal dichalchogenides, ACS Nano 11 (2017) 8242–8248.
[91] M.N. Blonsky, H.L. Zhuang, A.K. Singh, R.G. Hennig, Ab initio prediction of piezoelectricity in two-dimensional materials, ACS Nano 9 (2015) 9885–9891.
[92] Y. Chen, J. Liu, J. Yu, Y. Guo, Q. Sun, Symmetry-breaking induced large piezoelectricity in Janus tellurene materials, Phys. Chem. Chem. Phys. 21 (2019) 1207–1216.
[93] Y. Guo, H. Zhu, Q. Wang, Piezoelectric effects in surface-engineered two-dimensional group III nitrides, ACS Appl. Mater. Interfaces 11 (2018) 1033–1039.
[94] C. Cui, F. Xue, W.-J. Hu, L.-J. Li, Two-dimensional materials with piezoelectric and ferroelectric functionalities, npj 2D Mater. Appl. 2 (2018) 1–14.
[95] C. Cui, F. Xue, W.-J. Hu, L.-J. Li, Two-dimensional materials with piezoelectric and ferroelectric functionalities, npj 2D Mat. Appl. 2 (2018) 1–14.
[96] Y. Guo, J. Zhou, H. Xie, Y. Chen, Q. Wang, Screening transition metal-based polar pentagonal monolayers with large piezoelectricity and shift current, npj Comput. Mater. 8 (2022) 1–9.
[97] S.-D. Guo, X.-S. Guo, R.-Y. Han, Y. Deng, Predicted Janus SnSSe monolayer: a comprehensive first-principles study, Phys. Chem. Chem. Phys. 21 (2019) 24620–24628.
[98] S.-D. Guo, X.-S. Guo, Z.-Y. Liu, Y.-N. Quan, Large piezoelectric coefficients combined with high electron mobilities in Janus monolayer XTeI (X= Sb and Bi): a first-principles study, J. Appl. Phys. 127 (2020) 064302.
[99] M. Shahrokhi, Tuning the band gap and optical spectra of monolayer penta-graphene under in-plane biaxial strains, Optik 136 (2017) 205–214.
[100] L. Li, K. Jin, C. Du, X. Liu, The effect of oxidation on the electronic properties of penta-graphene: first-principles calculation, RSC Adv. 9 (2019) 8253–8261.
[101] J. Quijano-Briones, H. Fernández-Escamilla, A. Tlahuice-Flores, Doped penta-graphene and hydrogenation of its related structures: a structural and electronic DFT-D study, Phys. Chem. Chem. Phys. 18 (2016) 15505–15509.
[102] H. Alborznia, M. Naseri, N. Fatahi, Buckling strain effects on electronic and optical aspects of penta-graphene nanostructure, Superlattices Microstruct. 133 (2019) 106217.
[103] W.J. Lee, J. Lim, S.O. Kim, Nitrogen dopants in carbon nanomaterials: defects or a new opportunity? Small Methods 1 (2017) 1600014.
[104] G. Berdiyorov, G. Dixit, M. Madjet, Band gap engineering in penta-graphene by substitutional doping: first-principles calculations, J. Phys. Condens. Matter 28 (2016) 475001.
[105] R.M. Dos Santos, L.E. de Sousa, D.S. Galvão, L.A. Ribeiro, tuning penta-graphene electronic properties through engineered Line Defects, Sci. Rep. 10 (2020) 1–8.
[106] X. Dai, T. Shen, Y. Feng, H. Liu, Structure, electronic and optical properties of Al, Si, P doped penta-graphene: a first-principles study, Phys. B Condens. Matter 574 (2019) 411660.
[107] H. Einollahzadeh, S.M. Fazeli, R.S. Dariani, Studying the electronic and phononic structure of penta-graphane, Sci. Technol. Adv. Mater. 17 (2016) 610–617.
[108] O. Gritsenko, Ł. Mentel, E. Baerends, On the errors of local density (LDA) and generalized gradient (GGA) approximations to the Kohn-Sham potential and orbital energies, J. Chem. Phys. 144 (2016) 204114.
[109] J. Heyd, G.E. Scuseria, M. Ernzerhof, Hybrid functionals based on a screened Coulomb potential, J. Chem. Phys. 118 (2003) 8207–8215.
[110] H. Wang, T. Maiyalagan, X. Wang, Review on recent progress in nitrogen-doped graphene: synthesis, characterization, and its potential applications, ACS Catal. 2 (2012) 781–794.
[111] S. Agnoli, M. Favaro, Doping graphene with boron: a review of synthesis methods, physicochemical characterization, and emerging applications, J. Mater. Chem. A 4 (2016) 5002–5025.
[112] S.S. Chauhan, P. Srivastava, A.K. Shrivastava, Electronic and transport properties of boron and nitrogen doped graphene nanoribbons: an ab initio approach, Appl. Nanosci. 4 (2014) 461–467.
[113] J. Sturala, J. Luxa, M. Pumera, Z. Sofer, Chemistry of graphene derivatives: synthesis, applications, and perspectives, Chem. - Eur. J. 24 (2018) 5992–6006.
[114] Y. Zhang, J. Zhang, D.S. Su, Substitutional doping of carbon nanotubes with heteroatoms and their chemical applications, ChemSusChem 7 (2014) 1240–1250.
[115] N. Sathishkumar, S.Y. Wu, H.T. Chen, Boron-and nitrogen-doped penta-graphene as a promising material for hydrogen storage: a computational study, Int. J. Energy Res. 43 (2019) 4867–4878.
[116] L.-L. Liu, Y. Wang, C.-P. Chen, H.-X. Yu, L.-S. Zhao, X.-C. Wang, Tuning the electronic and magnetic properties of penta-graphene using a hydrogen atom: a theoretical study, RSC Adv. 7 (2017) 40200–40207.
[117] T.-T. Vu, V.-T. Tran, Tight-binding description for the electronic band structure of penta-graphene, Semicond. Sci. Technol. 35 (2020) 095037.
[118] J. Deb, N. Seriani, U. Sarkar, Ultrahigh carrier mobility of penta-graphene: a first-principle study, Phys. E Low-Dimens. Syst. Nanostruct. 127 (2021) 114507.
[119] J. Wang, Z. Wang, R. Zhang, Y. Zheng, L. Chen, S. Wang, C.-C. Tsoo, H.-J. Huang, W.-S. Su, A first-principles study of the electrically tunable band gap in few-layer penta-graphene, Phys. Chem. Chem. Phys. 20 (2018) 18110–18116.
[120] S. Guo, Y. Zhang, Y. Ge, S. Zhang, H. Zeng, H. Zhang, 2D V-V binary materials: status and challenges, Adv. Mater. 31 (2019) 1902352.
[121] S. Bruzzone, G. Fiori, Ab-initio simulations of deformation potentials and electron mobility in chemically modified graphene and two-dimensional hexagonal boron-nitride, Appl. Phys. Lett. 99 (2011) 222108.
[122] X. Peng, Q. Wei, G. Yang, Enhanced carrier mobility in anisotropic two-dimensional tetrahex-carbon through strain engineering, Carbon 165 (2020) 37–44.
[123] X. Li, Y. Dai, M. Li, W. Wei, B. Huang, Stable Si-based pentagonal monolayers: high carrier mobilities and applications in photocatalytic water splitting, J. Mater. Chem. A 3 (2015) 24055–24063.
[124] S. Sun, F. Meng, Y. Xu, J. He, Y. Ni, H. Wang, Flexible, auxetic and strain-tunable two dimensional penta-X_2C family as water splitting photocatalysts with high carrier mobility, J. Mater. Chem. A 7 (2019) 7791–7799.
[125] X. Li, H. Li, X. Zuo, L. Kang, D. Li, B. Cui, D. Liu, Chemically functionalized pentastanene monolayers for light harvesting with high carrier mobility, J. Phys. Chem. C 122 (2018) 21763–21769.
[126] A. Rawat, N. Jena, A. De Sarkar, A comprehensive study on carrier mobility and artificial photosynthetic properties in group VI B transition metal dichalcogenide monolayers, J. Mater. Chem. A 6 (2018) 8693–8704.
[127] V.K. Yadav, S.H. Mir, J.K. Singh, A computational study of structural, electronic and carrier mobility of boron and phosphorus/nitrogen co-doped graphene, Phys. B Condens. Matter 571 (2019) 291–295.
[128] H. Song, J. Liu, B. Liu, J. Wu, H.-M. Cheng, F. Kang, Two-dimensional materials for thermal management applications, Joule 2 (2018) 442–463.
[129] A.A. Balandin, S. Ghosh, W. Bao, I. Calizo, D. Teweldebrhan, F. Miao, C.N. Lau, Superior thermal conductivity of single-layer graphene, Nano Lett. 8 (2008) 902–907.
[130] D.L. Nika, E.P. Pokatilov, A.A. Balandin, Theoretical description of thermal transport in graphene: the issues of phonon cut-off frequencies and polarization branches, Phys. Status Solidi B 248 (2011) 2609–2614.
[131] Y.-Y. Zhang, Q.-X. Pei, Y. Cheng, Y.-W. Zhang, X. Zhang, Thermal conductivity of penta-graphene: the role of chemical functionalization, Comput. Mater. Sci. 137 (2017) 195–200.
[132] H. Liu, G. Qin, Y. Lin, M. Hu, Disparate strain dependent thermal conductivity of two-dimensional penta-structures, Nano Lett. 16 (2016) 3831–3842.

[133] H. Dong, Z. Zhang, Z. Feng, J. Kang, D. Wu, Q. Wang, J. Li, R. Su, Origins of low lattice thermal conductivity in 2D carbon allotropes, J. Mater. Res. Technol. 11 (2021) 1982–1990.

[134] Z. Sun, K. Yuan, X. Zhang, G. Qin, X. Gong, D. Tang, Disparate strain response of the thermal transport properties of bilayer penta-graphene as compared to that of monolayer penta-graphene, Phys. Chem. Chem. Phys. 21 (2019) 15647–15655.

[135] X.-K. Chen, K.-Q. Chen, Thermal transport of carbon nanomaterials, J. Phys. Condens. Matter 32 (2020) 153002.

[136] F.Q. Wang, J. Liu, X. Li, Q. Wang, Y. Kawazoe, Weak interlayer dependence of lattice thermal conductivity on stacking thickness of penta-graphene, Appl. Phys. Lett. 111 (2017) 192102.

[137] J. Sun, Y. Guo, Q. Wang, Y. Kawazoe, Thermal transport properties of penta-graphene with grain boundaries, Carbon 145 (2019) 445–451.

[138] X. Wu, V. Varshney, J. Lee, T. Zhang, J.L. Wohlwend, A.K. Roy, T. Luo, Hydrogenation of penta-graphene leads to unexpected large improvement in thermal conductivity, Nano Lett. 16 (2016) 3925–3935.

[139] X. Li, K. Maute, M.L. Dunn, R. Yang, Strain effects on the thermal conductivity of nanostructures, Phys. Rev. B 81 (2010) 245318.

[140] X. Gu, R. Yang, First-principles prediction of phononic thermal conductivity of silicene: a comparison with graphene, J. Appl. Phys. 117 (2015) 025102.

[141] W. Xu, L. Zhu, Y. Cai, G. Zhang, B. Li, Direction dependent thermal conductivity of monolayer phosphorene: parameterization of Stillinger-Weber potential and molecular dynamics study, J. Appl. Phys. 117 (2015) 214308.

[142] Y. Cai, J. Lan, G. Zhang, Y.-W. Zhang, Lattice vibrational modes and phonon thermal conductivity of monolayer MoS_2, Phys. Rev. B 89 (2014) 035438.

[143] Y. Zhao, P. Yu, G. Zhang, M. Sun, D. Chi, K. Hippalgaonkar, J.T. Thong, J. Wu, Low-symmetry $PdSe_2$ for high performance thermoelectric applications, Adv. Funct. Mater. 30 (2020) 2004896.

[144] H. Qin, C. Feng, X. Luan, D. Yang, First-principles investigation of adsorption behaviors of small molecules on penta-graphene, Nanoscale Res. Lett. 13 (2018) 1–7.

[145] C. Feng, X.-H. Luan, P. Zhang, J. Xiao, D.-G. Yang, H.-B. Qin, A first-principle study of the adsorption behavior of NO gas molecules on pristine and Al-doped penta-graphene, in: Proceedings of the 2017 18th International Conference on Electronic Packaging Technology (ICEPT), IEEE, 2017, pp. 1138–1142.

[146] R. Habibpour, A. Ahmadi, M. Faghihnasiri, P. Amani, A comparative investigation of penta-graphene and Pt single atom@ penta-graphene in H_2 and O_2 detection: DFT study with assessment of the van der Waals density functionals, Appl. Surf. Sci. 528 (2020) 147043.

[147] S.N. Talapaneni, G. Singh, I.Y. Kim, K. AlBahily, Aa.H. Al-Muhtaseb, A.S. Karakoti, E. Tavakkoli, A. Vinu, Nanostructured carbon nitrides for CO_2 capture and conversion, Adv. Mater. 32 (2020) 1904635.

[148] M. Wang, Z. Zhang, Y. Gong, S. Zhou, J. Wang, Z. Wang, S. Wei, W. Guo, X. Lu, Penta-graphene as a promising controllable CO_2 capture and separation material in an electric field, Appl. Surf. Sci. 502 (2020) 144067.

[149] C.-P. Zhang, B. Li, Z.-G. Shao, First-principle investigation of CO and CO_2 adsorption on Fe-doped penta-graphene, Appl. Surf. Sci. 469 (2019) 641–646.

[150] N. Sathishkumar, S.-Y. Wu, H.-T. Chen, Charge-modulated/electric-field controlled reversible CO_2/H_2 capture and storage on metal-free N-doped penta-graphene, Chem. Eng. J. 391 (2020) 123577.

[151] X. Lu, M. Wang, G. Luo, S. Zhou, J. Wang, H. Xin, Z. Wang, S. Liu, S. Wei, High-efficiency CO_2 capture and separation over N_2 in penta-graphene pores: insights from GCMC and DFT simulations, J. Mater. Sci. 55 (2020) 16603–16611.

[152] G. Sdanghi, R.L. Canevesi, A. Celzard, M. Thommes, V. Fierro, Characterization of carbon materials for hydrogen storage and compression, Chin. J. Carbon Res. 6 (2020) 46.

[153] N.C. Gallego, T.D. Burchell, A.M. Clark, Carbon materials for hydrogen storage, Carbon (2004) 11–16.

[154] H.-S. Jang, J. Mun, W.G. Hong, S.M. Lee, J.W. Jeon, C.Y. Lee, H.J. Kim, B.H. Kim, The performance of green carbon as a backbone for hydrogen storage materials, Int. J. Hydrog. Energy 45 (2020) 10516–10522.

[155] V. Tozzini, V. Pellegrini, Prospects for hydrogen storage in graphene, Phys. Chem. Chem. Phys. 15 (2013) 80–89.

[156] A.G. Klechikov, G. Mercier, P. Merino, S. Blanco, C. Merino, A.V. Talyzin, Hydrogen storage in bulk graphene-related materials, Microporous Mesoporous Mater. 210 (2015) 46–51.

[157] A. Ngqalakwezi, D. Nkazi, G. Seifert, T. Ntho, Effects of reduction of graphene oxide on the hydrogen storage capacities of metal graphene nanocomposite, Catal. Today 358 (2020) 338–344.

[158] N. Zheng, S. Yang, H. Xu, Z. Lan, Z. Wang, H. Gu, A DFT study of the enhanced hydrogen storage performance of the Li-decorated graphene nanoribbons, Vacuum 171 (2020) 109011.

[159] M. Mohan, V.K. Sharma, E.A. Kumar, V. Gayathri, Hydrogen storage in carbon materials—a review, Energy Storage 1 (2019) e35.

[160] R. Ströbel, J. Garche, P. Moseley, L. Jörissen, G. Wolf, Hydrogen storage by carbon materials, J. Power Sources 159 (2006) 781–801.

[161] J.-H. Guo, X.-D. Li, X.-L. Cheng, H.-Y. Liu, S.-J. Li, G. Chen, The theoretical study of the bimetallic Ni/Pd, Ni/Pt and Pt/Pd catalysts for hydrogen spillover on penta-graphene, Int. J. Hydrog. Energy 43 (2018) 19121–19129.

[162] J.-H. Guo, D.-D. Liu, X.-D. Li, H.-Y. Liu, G. Chen, Pt_4, Pd_4, Ni_4, and Ti_4 catalyzed hydrogen spillover on penta-graphene for hydrogen storage: the first-principles and kinetic Monte Carlo study, Int. J. Hydrog. Energy 43 (2018) 2247–2255.

[163] D. Deng, K. Novoselov, Q. Fu, N. Zheng, Z. Tian, X. Bao, Catalysis with two-dimensional materials and their heterostructures, Nat. Nanotechnol. 11 (2016) 218–230.

[164] Z.-P. Liu, P. Hu, A. Alavi, Catalytic role of gold in gold-based catalysts: a density functional theory study on the CO oxidation on gold, J. Am. Chem. Soc. 124 (2002) 14770–14779.

[165] X.-Q. Gong, Z.-P. Liu, R. Raval, P. Hu, A systematic study of CO oxidation on metals and metal oxides: density functional theory calculations, J. Am. Chem. Soc. 126 (2004) 8–9.

[166] R. Krishnan, S.-Y. Wu, H.-T. Chen, Nitrogen-doped penta-graphene as a superior catalytic activity for CO oxidation, Carbon 132 (2018) 257–262.

[167] R. Krishnan, S.-Y. Wu, H.-T. Chen, Catalytic CO oxidation on B-doped and BN co-doped penta-graphene: a computational study, Phys. Chem. Chem. Phys. 20 (2018) 26414–26421.

[168] R. Krishnan, S.-Y. Wu, H.-T. Chen, Single Pt atom supported on penta-graphene as an efficient catalyst for CO oxidation, Phys. Chem. Chem. Phys. 21 (2019) 12201–12208.

[169] D. Li, W. Li, J. Zhang, Catalytic CO oxidation by Fe doped penta-graphene: a density functional study, Mol. Catal. 470 (2019) 48–55.

[170] K. Choudhary, K.F. Garrity, G. Pilania, F. Tavazza, Efficient Computational Design of 2D van der Waals Heterostructures: Band-alignment, Lattice-mismatch, Web-app Generation and Machine-learning, arXiv prep. arXiv:2004.03025, 2020.

[171] K. Zhao, Y. Guo, Q. Wang, Contact properties of a vdW heterostructure composed of penta-graphene and penta-BN_2 sheets, J. Appl. Phys. 124 (2018) 165103.

[172] J. Li, X. Fan, Y. Wei, G. Chen, Penta-B_xN_y sheet: a density functional theory study of two-dimensional material, Sci. Rep. 6 (2016) 1–9.

[173] Q. Chen, M.-Q. Cheng, K. Yang, W.-Q. Huang, W. Hu, G.-F. Huang, Dispersive and covalent interactions in all-carbon heterostructures consisting of penta-graphene and fullerene: topological effect, J. Phys. D Appl. Phys. 51 (2018) 305301.

[174] X. Yi, M. Long, A. Liu, S. Zhang, M. Li, H. Xu, Study on electronic structures and transport properties of penta-graphene and penta-B_2N_4 heterojunctions, Phys. B Condens. Matter 595 (2020) 412362.

[175] X. Yi, M. Long, A. Liu, S. Zhang, M. Li, H. Xu, Study on electronic structures and transport properties of penta-graphene and penta-B_2N_4 heterojunctions, Phys. B Condens. Matter 595 (2020) 412362.

[176] A. Hassan, Y. Guo, Q. Wang, Y. Kawazoe, P. Jena, Interfacial properties of penta-graphene-metal contacts, J. Appl. Phys. 125 (2019) 065308.

[177] X. Zhang, J. Hu, Y. Cheng, H.Y. Yang, Y. Yao, S.A. Yang, Borophene as an extremely high capacity electrode material for Li-ion and Na-ion batteries, Nanoscale 8 (2016) 15340–15347.

[178] B. Mortazavi, A. Dianat, G. Cuniberti, T. Rabczuk, Application of silicene, germanene and stanene for Na or Li ion storage: a theoretical investigation, Electrochim. Acta 213 (2016) 865–870.

[179] Q. Sun, Y. Dai, Y. Ma, T. Jing, W. Wei, B. Huang, Ab initio prediction and characterization of Mo_2C monolayer as anodes for lithium-ion and sodium-ion batteries, J. Phys. Chem. Lett. 7 (2016) 937–943.

[180] R.-S. Meng, M. Cai, J.-K. Jiang, Q.-H. Liang, X. Sun, Q. Yang, C.-J. Tan, X.-P. Chen, First principles investigation of small molecules adsorption on antimonene, IEEE Electron Device Lett. 38 (2016) 134–137.

[181] M.-Q. Cheng, Q. Chen, K. Yang, W.-Q. Huang, W.-Y. Hu, G.-F. Huang, Penta-graphene as a potential gas sensor for NO_x detection, Nanoscale Res. Lett. 14 (2019) 1–8.

[182] O. Leenaerts, B. Partoens, F. Peeters, Adsorption of H_2O, NH_3, CO, NO_2, and NO on graphene: a first-principles study, Phys. Rev. B 77 (2008) 125416.

[183] L. Kou, T. Frauenheim, C. Chen, Phosphorene as a superior gas sensor: selective adsorption and distinct I–V response, J. Phys. Chem. Lett. 5 (2014) 2675–2681.

[184] Y. Li, P. Yuan, Z. Fan, Z. Zhang, Electronic properties and carrier mobility for penta-graphene nanoribbons with nonmetallic-atom-terminations, Org. Electron. 59 (2018) 306–313.

[185] J.M. de Sousa, G. Brunetto, V.R. Coluci, D.S. Galvao, Torsional "superplasticity" of graphyne nanotubes, Carbon 96 (2016) 14–19.

[186] M. Dresselhaus, G. Dresselhaus, R. Saito, Physics of carbon nanotubes, Carbon 33 (1995) 883–891.

[187] Q. Guo, Y. Xie, X. Wang, S. Zhang, T. Hou, S. Lv, Synthesis of carbon nitride nanotubes with the C_3N_4 stoichiometry via a benzene-thermal process at low temperatures, Chem. Commun. (2004) 26–27.

[188] J. De Sousa, A. Aguiar, E. Girão, A.F. Fonseca, V. Coluci, D. Galvão, Elastic and Fracture Properties of Single Walled Pentagraphene Nanotubes, arXiv prep. arXiv:1911.12251, 2019.

[189] H. Wang, N. Ding, T. Jiang, F. Zhang, X. Zhao, W. Liu, F. Zaïri, Investigation on electronic and mechanical properties of penta-graphene nanotubes, J. Mater. Sci. 55 (2020) 14336–14344.

[190] J. Quijano-Briones, H. Fernández-Escamilla, A. Tlahuice-Flores, Chiral penta-graphene nanotubes: structure, bonding and electronic properties, Comput. Theor. Chem. 1108 (2017) 70–75.

[191] P. Avramov, V. Demin, M. Luo, C.H. Choi, P.B. Sorokin, B. Yakobson, L. Chernozatonskii, Translation symmetry breakdown in low-dimensional lattices of pentagonal rings, J. Phys. Chem. Lett. 6 (2015) 4525–4531.

[192] J. De Sousa, A. Aguiar, E. Girão, A.F. Fonseca, V. Coluci, D. Galvão, Mechanical properties of single-walled penta-graphene-based nanotubes: a DFT and classical molecular dynamics study, Chem. Phys. 547 (2021) 111187.

[193] J. De Sousa, T. Botari, E. Perim, R. Bizao, D.S. Galvao, Mechanical and structural properties of graphene-like carbon nitride sheets, RSC Adv. 6 (2016) 76915–76921.

[194] J.M. De Sousa, A.L. Aguiar, E.C. Girão, A.F. Fonseca, A. Souza Filho, D.S. Galvao, Mechanical properties of pentagraphene-based nanotubes: a molecular dynamics study, MRS Adv. 3 (2018) 97–102.

[195] M. Chen, H. Zhan, Y. Zhu, H. Wu, Y. Gu, Mechanical properties of penta-graphene nanotubes, J. Phys. Chem. C 121 (2017) 9642–9647.
[196] V. Popov, V. Van Doren, M. Balkanski, Elastic properties of single-walled carbon nanotubes, Phys. Rev. B 61 (2000) 3078.
[197] Z. Wang, X. Cao, C. Qiao, R. Zhang, Y. Zheng, L. Chen, S. Wang, C.-Z. Wang, K.-M. Ho, Y.-J. Fan, Novel penta-graphene nanotubes: strain-induced structural and semiconductor–metal transitions, Nanoscale 9 (2017) 19310–19317.
[198] T. Wu, M. Yao, J. Li, M. Li, M. Long, First-principles prediction of the electronic property, carrier mobility and optical absorption in edge-modified pristine sawtooth penta-graphene nanoribbons (SSPGNRs), Results Phys. 17 (2020) 103103.
[199] C. He, X. Wang, W. Zhang, Coupling effects of the electric field and bending on the electronic and magnetic properties of penta-graphene nanoribbons, Phys. Chem. Chem. Phys. 19 (2017) 18426–18433.
[200] K. Tarawneh, Density Functional Theory Studies of Vacancies in Penta-Graphene Nanoribbons, in: Proceedings of the Advances in Science and Engineering Technology International Conferences (ASET), IEEE, pp. 1–4.
[201] H. Liu, A.T. Neal, Z. Zhu, Z. Luo, X. Xu, D. Tománek, P.D. Ye, Phosphorene: an unexplored 2D semiconductor with a high hole mobility, ACS Nano 8 (2014) 4033–4041.
[202] S. Ghosh, W. Bao, D.L. Nika, S. Subrina, E.P. Pokatilov, C.N. Lau, A.A. Balandin, Dimensional crossover of thermal transport in few-layer graphene, Nat. Mater. 9 (2010) 555–558.
[203] X. Zhu, H. Su, Chiral pentagon only diamond-like structures, J. Phys. Chem. C 121 (2017) 13810–13815.
[204] Y. Fujii, M. Maruyama, N.T. Cuong, S. Okada, Pentadiamond: a hard carbon allotrope of a pentagonal network of sp^2 and sp^3 C atoms, Phys. Rev. Lett. 125 (2020) 016001.
[205] R.M. Tromer, L.C. Felix, C.F. Woellner, D.S. Galvao, A DFT investigation of the electronic, optical, and thermoelectric properties of pentadiamond, Chem. Phys. Lett. 763 (2021) 138210.
[206] B. Mortazavi, F. Shojaei, X. Zhuang, L.F.C. Pereira, First-principles investigation of electronic, optical, mechanical and heat transport properties of pentadiamond: a comparison with diamond, Carbon Trends 3 (2021) 100036.
[207] P.-P. Sun, D.R. Kripalani, L. Bai, W. Chi, K. Zhou, Pentadiamond: a highly efficient electron transport layer for perovskite solar cells, J. Phys. Chem. C 125 (2021) 5372–5379.
[208] V. Brazhkin, M. Kondrin, A. Kvashnin, E. Mazhnik, A. Oganov, Comment on" Pentadiamond: A Hard Carbon Allotrope of a Pentagonal Network of sp2 and sp3 atoms", arXiv prep. arXiv:2007.08912, 2020.
[209] Y. Fujii, M. Maruyama, N.T. Cuong, S. Okada, Retraction: pentadiamond: a hard carbon allotrope of a pentagonal network of sp^2 and sp3C atoms [Phys. Rev. Lett. 125, 016001 (2020)], Phys. Rev. Lett. 125 (2020) 079901.
[210] H. Qin, G. Zhang, Y. Zhang, L. Qin, Y. Liu, Q.-X. Pei, Temperature and defect effects on the mechanical properties of pentadiamond, Diam. Relat. Mater. 118 (2021) 108523.
[211] L.C. Felix, R.M. Tromer, C.F. Woellner, C.S. Tiwary, D.S. Galvao, Mechanical Response of Pentadiamond: A DFT and Molecular Dynamics Study, arXiv prep. arXiv:2105.02335, 2021.
[212] Y. Chen, J. Sun, T. Li, Q. Wang, Low lattice thermal conductivity of pentadiamond, J. Appl. Phys. 129 (2021) 215107.
[213] S. Cahangirov, M. Topsakal, E. Aktürk, H. Şahin, S. Ciraci, Two-and one-dimensional honeycomb structures of silicon and germanium, Phys. Rev. Lett. 102 (2009) 236804.
[214] H. Okamoto, Y. Kumai, Y. Sugiyama, T. Mitsuoka, K. Nakanishi, T. Ohta, H. Nozaki, S. Yamaguchi, S. Shirai, H. Nakano, Silicon nanosheets and their self-assembled regular stacking structure, J. Am. Chem. Soc. 132 (2010) 2710–2718.
[215] D. Wu, S. Wang, S. Zhang, Y. Liu, Y. Ding, B. Yang, H. Chen, Stabilization of two-dimensional penta-silicene for flexible lithium-ion battery anodes via surface chemistry reconfiguration, Phys. Chem. Chem. Phys. 21 (2019) 1029–1037.
[216] Y. Ding, Y. Wang, Hydrogen-induced stabilization and tunable electronic structures of penta-silicene: a computational study, J. Mater. Chem. C 3 (2015) 11341–11348.
[217] D. Wu, S. Wang, S. Zhang, Y. Liu, Y. Ding, B. Yang, H. Chen, Stabilization of two-dimensional penta-silicene for flexible lithium-ion battery anodes via surface chemistry reconfiguration, Phys. Chem. Chem. Phys. 21 (2019) 1029–1037.
[218] Y. Aierken, O. Leenaerts, F.M. Peeters, A first-principles study of stable few-layer penta-silicene, Phys. Chem. Chem. Phys. 18 (2016) 18486–18492.
[219] S. Sheng, R. Ma, J.-b. Wu, W. Li, L. Kong, X. Cong, D. Cao, W. Hu, J. Gou, J.-W. Luo, The pentagonal nature of self-assembled silicon chains and magic clusters on Ag (110), Nano Lett. 18 (2018) 2937–2942.
[220] Y. Guo, C. Zhang, J. Zhou, Q. Wang, P. Jena, Lattice dynamic and instability in pentasilicene: a light single-element ferroelectric material with high curie temperature, Phys. Rev. Appl. 11 (2019) 064063.
[221] Z. Gao, Z. Zhang, G. Liu, J.-S. Wang, Ultra-low lattice thermal conductivity of monolayer penta-silicene and penta-germanene, Phys. Chem. Chem. Phys. 21 (2019) 26033–26040.
[222] Z. Gao, J.-S. Wang, Thermoelectric penta-silicene with a high room-temperature figure of merit, ACS Appl. Mater. Interfaces 12 (2020) 14298–14307.
[223] K. Kurosaki, S.-a. Tanusilp, Development of Si-based high efficiency thermoelectric materials, Impact 2018 (2018) 21–23.
[224] M. Dávila, L. Xian, S. Cahangirov, A. Rubio, G. Le Lay, Germanene: a novel two-dimensional germanium allotrope akin to graphene and silicene, New J. Phys. 16 (2014) 095002.
[225] J. Zhao, H. Zeng, Chemical functionalization of pentagermanene leads to stabilization and tunable electronic properties by external tensile strain, ACS Omega 2 (2017) 171–180.

Muhammad Azhar Nazir received his M.S. degree (2020) in Materials Science from the University of Lahore, Pakistan. Currently, he is pursuing his P.hD degree under the supervision of Prof. Qian Wang at the School of Materials Science and Engineering, Peking University. His current research interests include the design of low-dimensional carbon materials and the study of pentagon-based heterostructures for a variety of applications.

Arzoo Hassan has received her MSc. degree in physics from International Islamic University Islamabad, Pakistan. Currently, she is doing Ph.D. under the supervision of Prof. Wang Qian at School of Materials Science and Engineering, Peking University. Her current research focuses on design and properties of novel-2D semiconductors/metal heterojunctions using first-principles calculations and finds their applications in FET devices and secondary ion batteries. She is also a Co-founder & CAO of WEmpower Pakistan.

Yiheng Shen received his B. E. degree in materials science and engineering from Peking university (PKU) in 2018. Now he is a Ph.D. candidate in Prof. Qian Wang's group at the School of Materials Science and Engineering, PKU. His current research focuses on the design and properties of pentagon-based materials.

Qian Wang is a full Professor at the School of Materials Science and Engineering, Peking University. She earned a PhD degree from Tohoku University (Japan) in 2001. Her current research interests include computational design and theoretical study of carbon materials and pentagon-based functional materials for spintronics, thermoelectricity, piezoelectricity, battery anodes, and heterojunctions. She has been selected among the "Most Cited Chinese Researchers" every year since 2014, and won the IAAM Medal issued by International Association of Advanced Materials for her contribution to "Carbon Materials and Technology" in 2021.